Ionizing Radiation Sensitivity of Hydroxyl Terminated Polybutadiene Solid Propellant

A Dissertation

Presented in Partial Fulfillment of the Requirements for the

Degree of Doctor of Philosophy

with a

Major in Mechanical Engineering

in the

College of Graduate Studies

University of Idaho

by

Juan Carlos Lopez

Major Professor: John C. Crepeau, Ph.D., P.E.;

Committee Members: Ralph S. Budwig, Ph.D.; P.E., Kamal Kumar, Ph.D.;

Indrajit Charit, Ph.D., P.E.;

Department Administrator: Steven Beyerlein, Ph.D.

August 2019

Authorization to Submit Dissertation

This dissertation of Juan Carlos Lopez submitted for the degree of Doctor of Philosophy with a major in Mechanical Engineering and titled "Ionizing Radiation Sensitivity of Hydroxyl Terminated Polybutadiene Solid Propellant" has been reviewed in final form, as indicated by the signatures and dates given below. Permission is now granted to submit copies to the College of Graduate Studies for approval.

Major Professor: _____ Date: _____
John C. Crepeau, Ph.D., P.E.

Committee Members: _____ Date: _____
Ralph S. Budwig, Ph.D., P.E.

_____ Date: _____
Kamal Kumar, Ph.D.

_____ Date: _____
Indrajit Charit, Ph.D., P.E.

Department Administrator: _____ Date: _____
Steven Beyerlein, Ph.D.

Abstract

The effects of ionizing radiation on hydroxyl-terminated polybutadiene (HTPB) solid propellant are investigated to assess its sensitivity to electron radiation. Investigation into the radiation sensitivity of HTPB propellant is needed to assess potential risks to a mission aimed at landing a craft on the surface of Jupiter's moon Europa, considering this region of space has very high particle radiation fields. This mission would require deploying a Europa Breaking Motor (EBM) using HTPB propellant to provide the necessary deceleration to safely land a craft on Europa's icy surface. The current concept for an EBM requires motor components, including the propellant, to have a radiation sensitivity of no less than 2.4 Mrad.

While HTPB solid propellant has been studied and used in rockets to place satellites in orbit and for military applications, it has not been previously investigated to support, with sufficient confidence, missions to Jupiter's moons. Tensile data from surrogate propellant, binder, hybrid propellant and HTPB propellant are used to derive values for radiation sensitivity on the basis of crosslink density, particle adhesion, debonding and damage to the aluminum and ammonium perchlorate. Using the Flory – Rehner and Mooney – Rivlin models, the propellant's limiting value for crosslink density is computed with its corresponding radiation dose. The Pukansky model is used here to obtain a limiting value for the propellant bonding factor and its corresponding radiation dose. Similarly, the Nicolasis – Narkis model is use to derive values for the propellant's particle adhesion factor and its corresponding radiation dose. Lastly, the Goodier model is applied to derive the maximum load on the aluminum and ammonium perchlorate in the propellant with their corresponding radiation dose. The computed values for radiation dose obtained from these models were then compared to the radiation sensitivity value for the EBM components of 2.4 Mrad. The results from these models show ammonium perchlorate to have a radiation sensitivity that does not amply support the current motor concept in relation to the 2.4 Mrad requirement. This, in turn, necessitates further refinement of the EBM design to possibly provide shielding in the case liner for the propellant.

Acknowledgements

I thank Professor John C. Crepeau, Ph.D., P.E., at the University of Idaho, whose vision and passion for education made this work possible. Overcoming the challenges needed to bring this effort to fruition is testament to his wealth of knowledge in the application of science and of gaining greater understanding of our place in the universe.

I thank the members of my Doctoral Committee, Professor Kamal Kumar, Ph.D., Professor Indrajit Charit, Ph.D., P.E., and Professor Ralph Budwig, Ph.D., P.E. Your invaluable support has enabled me to experience the rewards of life-long learning through challenge, discovery and contribution to our noble profession.

I thank the members of the Europa team at Marshall Space Flight Center who facilitated resources and knowledge, enabling me to learn and to have the privilege of sharing experiences with some of our nation's brightest professionals whose quest for scientific exploration is a bright light in the vastness of space.

A special thanks to Professor Steven Beyerlein, Ph.D., Chairman of the Department of Mechanical Engineering at the University of Idaho who, with Professor Crepeau, mobilized the necessary resources and departmental processes, so as to enable this work to take form, produce results, and affirm the valued relationship between NASA and the University of Idaho.

Dedication

To my wife, Francie, whose love has been my greatest blessing.

Table of Contents

List of Tables

List of Figures

List of Abbreviations

Al	Aluminum (particles)
ANOVA	Analysis of Variance
AP	Ammonium Perchlorate (oxidizer)
APL	Advanced Physics Lab (JHU)
AS	Ammonium Sulfate (surrogate)
DOE	Design of Experiment
EBM	Europa Braking Motor
EIS	Europa Imaging System, Johns Hopkins University-APL
EM41	Electrostatic MeV (Pelletron accelerator 41)
ESA	European Space Agency
ESTAR	Electron Stopping Power & Range
E-THEMIS	Europa Thermal Emission Imaging System, Arizona State University
F (ANOVA)	F-statistic (or F value)
FTIR	Fourier Transform Infra-red (spectroscopy)
HTPB	Hydroxyl-terminated Polybutadiene (Resin)
HX-752	Methyl aziridine (crosslinker & bonding agent)
I	Irradiated
ICEMAG	Interior Characterization of Europa using Magnetometry
IPDI	Isophorone Diisocyanate (curing agent & hardener)
JANNAF	Joint Army, Navy, NASA, Air Force (Specimen Geometry)
JHU	Johns Hopkins University (APL)
JPL	Jet Propulsion Laboratory, Pasadena, CA
JSC	NASA Johnson Space Center, Houston, TX
keV	kilo-electron Volt
kN	kilo Newton (224.81 pounds)
LLC	Limited Liability Company/Corporation
MASPEX	Mass Spectrometer for Planetary Exploration, Southwest Research Inst.
MeV	Mega-electron Volt

MISE	Mapping Imaging Spectrometer for Europa, NASA Jet Propulsion Lab
MONSOL	Monte Carlo Solver (model)
MS (ANOVA)	Mean of Squares
MSFC	Marshall Space Flight Center, Redstone Arsenal, AL
MTS	Materials Test Systems Co., Eden Prairie, MN
NASA	National Aeronautics & Space Administration
NIST	National Institute of Standards
NMR	(1H) Nuclear Magnetic Resonance (spectrometry)
PC	Pathfinder Control (Hybrid sample)
PIMS	Plasma Instrument for Magnetic Sounding
PMMA	Polymethyl methacrylate
PP	Polypropylene
ppm	parts per million
psi	pounds per square inch
R45	Resin 45 (HTPB grade/type)
REASON	Radar for Europa Assessment & Sounding: Ocean to Near Surface
R_J	Radius of Jupiter (71,492 km)
RTG	Radioisotope Thermal Nuclear Generator (Pioneer 10 mission)
SEM	Scanning Electron Microscope
SEP	Solar Energetic Particle
SETI	Search for Extraterrestrial Intelligence, University of California, Berkeley
SOFTLAND	Low Cost, Controllable Solid Martian Descent Stage (computer program)
SS (ANOVA)	Sum of Squares
SUDA	Surface Dust Mass Analyzer, University of Colorado, Boulder
UHF	Ultra-high Frequency
UI	Unirradiated
USA	United States of America
UVS	Ultraviolet Spectrograph-Europa, Southwest Research Institute
XRD	X-ray Diffraction

List of Symbols

Y_{stress}	Yield stress (psi)
Y_{strain}	Yield strain (%)
C_4H_6	trans-Butadiene
R_J	Radius (Jupiter)
$(OH)_n$	Hydroxyl Group(s)
NH_4ClO_4	Ammonium Perchlorate
$(C_4H_6)_n$	Polybutadiene
$(NH_4)_2SO_4$	Ammonium Sulfate
F (ANOVA)	Test Statistic
P (ANOVA)	Value of statistical significance
σ	Stress
V_p	Volume of (particle) filler
σ_c	Tensile stress of the composite
σ_m	Tensile stress of the matrix
σ'_p	Particle Load (corrected)
R	Universal gas constant
T	Temperature
C_1	Mooney – Rivlin crosslink density Gaussian term
C_2	Mooney – Rivlin crosslink density non-Gaussian term
ƛ	Extension ratio
V_e	Crosslink density
B	Particle/matrix reinforcement parameter
K	Adhesion parameter between filler particles and matrix

Chapter 1. Introduction

Deep space exploration requires an understanding of the effects of electron radiation on Hydroxyl-terminated Polybutadiene (HTPB) propellant as it is planned for use in the de-orbit stage for missions to Jupiter's moon Europa. Tensile data and Scanning Electron Microscope (SEM) scans from binder, hybrid and propellant specimens were used to assess the radiation sensitivity of HTPB propellant. The radiation sensitivity of the propellant is studied in relation to (1) molecular structure of the binder; (2) change in load bearing capacity of the aluminum and ammonium perchlorate particles; and (3) particle debonding. A glossary of the more commonly used terms in this dissertation is included in Appendix A.

The methodology for this dissertation relies on the use of I-bone specimens from three inert formulations before evaluating the propellant. These inert formulations consist of (1) binder only, (2) binder with aluminum, and (3) binder with aluminum and ammonium sulfate. There are three principal reasons for evaluating these inert formulations prior to evaluating the propellant. First, tensile testing of unirradiated and irradiated binder provided important values for Y_{stress} and Y_{strain} needed for modeling the crosslink density, modeling the load carried by the particles and modeling adhesion and bonding. Second, tensile testing of unirradiated and irradiated hybrid, which consists of binder and aluminum, provided insight as to how the presence of metallic particles change Y_{stress} and Y_{strain} values. Third, the use of a propellant surrogate provided insight of how changing the quantity of ingredients affect Y_{stress} and Y_{strain} values. Also, surrogate tests provided a way of identifying a range of Y_{stress} and Y_{strain} values necessary for the crosslink density models and for modeling the max load on the particles.

SEM scans of unirradiated and irradiated surrogate material also served to visually assess changes in morphology and particle debonding. Another important step prior to evaluating data from propellant specimens consisted of establishing the effects that could be investigated using tensile data noting that not all radiation effects on molecular structure are candidates for investigation using tensile data. To that end, this investigation focuses on crosslink density, particle load and debonding. The literature

search revealed that for the formulation and models available it would be necessary to identify Y_{stress} and Y_{strain} values for the binder. Investigations into the performance of the binder led to further investigations with binder and aluminum particles to determine how the addition of particles changes the mechanical performance of the binder. From minimum values for propellant Y_{stress} and Y_{strain}, computations for maximum crosslinking, particle loading and particle bonding and adhesion were conducted and compared against those values corresponding to a 6 Mrad reference dose. These values provided the basis for comparing the effects of electron radiation and determining the radiation sensitivity of each of the aforementioned three propellant characteristics. Establishing the radiation sensitivity required combining the results from pull tests, SEM scans and modeling, all culminating in graphical comparisons for each of the three major propellant characteristics.

As mentioned previously, analyses were performed on unirradiated and irradiated specimens for the binder, then binder with aluminum particles (referred to as hybrid) and propellant. Due to safety concerns, SEM scans were performed on unirradiated and irradiated binder and hybrid specimens but not on propellant. For irradiated specimens, a reference dose of 6 Mrad was delivered with a Pelletron generating electrons with a 2 MeV reference energy. The energy that is deposited in the propellant from electrons is of considerable interest in support of missions to Europa. This is because in addition to the 2.4 Mrad limit imposed by the design of the Europa Breaking Motor (EBM), high energy electrons are abundant and their energetic interactions could damage the propellant altering its burn rate and its performance.

While tensile specimens of the surrogate were not irradiated and tested, a small sample of surrogate was exposed to a very high radiation dose, which showed the ammonium sulfate experiencing cleavage at about 32 Mrad. The cleavage, or tearing, of the ammonium sulfate particles occurred at a higher dose than ammonium perchlorate, which is between 5 and 16 Mrad in the absence of mechanical forces. The results of mechanical tests of unirradiated surrogate specimens were evaluated using Analysis of

Variance to determine which ingredients have the more significant impact on Y_{stress} and Y_{strain}.

Ultimately, this analysis augments efforts to determine how electron radiation, which is abundant around Jupiter and its moons, could affect the burn rate of the propellant. The burn rate is dependent on the distribution and bonding of particles in the propellant. If the propellant's ability to maintain the oxidizer and fuel particles in place is reduced, this could lead to a potential reduction in motor performance.

1.1 Objective

This work was conducted for the purpose of building an understanding of HTPB solid propellant behavior following exposure to nuclear radiation using an electron accelerator. This analysis supports the planning phase for a future Europa mission to provide greater understanding about propellant performance and stability. Ultimately, this analysis augments efforts to determine how ionizing radiation changes the propellant's chemical properties respective of different mechanisms that include the network of crosslinks and chain extensions and how the effects on the fuel and oxidizer particles are significant when establishing the radiation sensitivity of the propellant. The results of this investigation will provide additional insight to recent efforts at the National Aeronautics & Space Administration (NASA) George C. Marshall Space Flight Center (MSFC) related to damage of ammonium perchlorate in the absence of mechanical forces. The collective knowledge set of this investigation and work on ammonium perchlorate will also aid in efforts to determine options and methods for further radiation testing in support of a Europa Lander project (Hattar, et al., 2017).

1.2 Problem Statement

Investigation into the radiation sensitivity of HTPB propellant is needed to assess potential risks to a mission aimed at landing a craft on the surface of Jupiter's moon Europa, considering this region of space has very high particle radiation fields. This mission would require deploying a Europa Breaking Motor (EBM) using HTPB propellant to provide the necessary deceleration to safely land a craft on Europa's icy surface.

However, if the propellant is overexposed to electron radiation the combined effects of the radiation with the mechanical forces that will be experienced at different stages of the journey could alter the propellant's burn rate in a manner that could cause the EBM to underperform. Previous investigation into the radiation sensitivity of the ammonium perchlorate in the absence of mechanical forces showed damage beginning at 5 Mrad with significant damage at 16 Mrad (Miloshevsky, et al., 2017). However, these values are in the absence of mechanical forces where debonding and friction between particles are not considered in relation to the radiation dose causing damage to the propellant. Therefore, it is necessary to assess the radiation sensitivity of the propellant in the presence of electron radiation and mechanical forces to determine if the propellant's radiation sensitivity exceeds the foreseeable radiation dose for the EBM components and if this will drive changes to the motor design.

1.3 Dissertation Organization

This investigation is structured to expand the body of knowledge for radiation sensitivity of HTPB solid propellant by determining which of its three main characteristics, consisting of crosslinking, particle stability and debonding, is the more radiation sensitive. As shown in **Figure 1.1**, a six-step process using unirradiated (UI) and irradiated (I) specimens was employed to determine propellant radiation sensitivity.

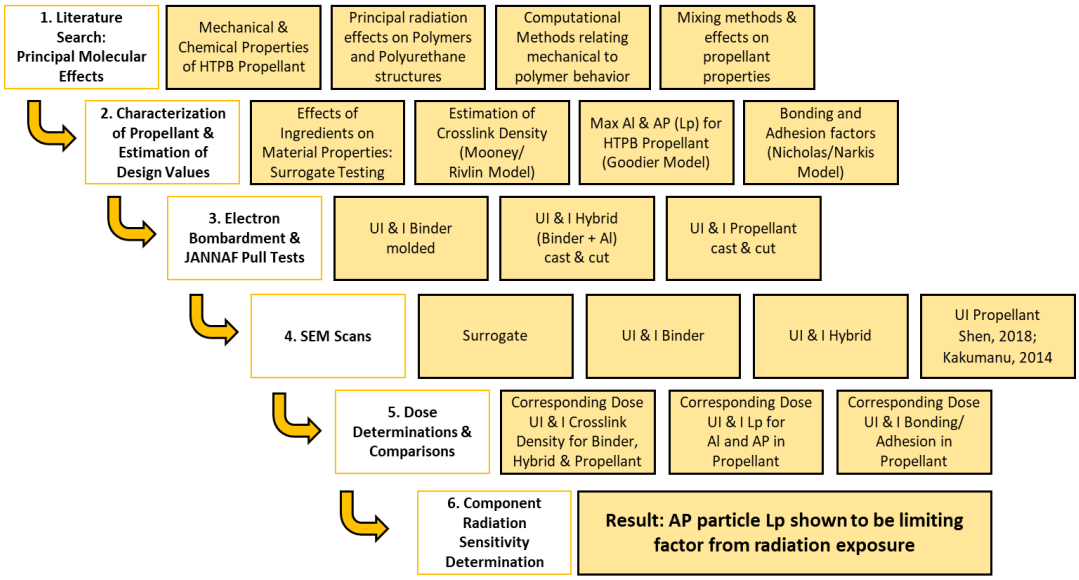

Figure 1.1: Methodology

This dissertation is organized in a manner that shows how data from tensile tests for standard Joint Army Navy NASA Air Force (JANNAF) specimens are used to determine the corresponding radiation dose from Y_{stress} and Y_{strain} values. Early in the literature survey, an essential part of this investigation, crosslinking and particle debonding were identified as important considerations in relation to radiation effects. To that end, it was important before the onset of any irradiation experiments, to investigate the effects that the basic ingredients in the propellant have on Y_{stress} and Y_{strain} and how these could in turn shed light on the importance of crosslinking and particle bonding. To accomplish this, it became necessary to develop a surrogate material that would provide the ability to test a large quantity of specimens without the safety risks from working with large quantities of actual propellant. Looking into possible models for particle composites revealed that it would be necessary to obtain Y_{stress} and Y_{strain} values for the binder alone. Several unsuccessful attempts were made to cast JANNAF specimens for the binder. The material proved to be impractical to cut so it became necessary to fabricate a mold. The mold proved successful in making JANNAF specimens for the binder. Before investigating the propellant, tests were performed by first adding aluminum particles to the binder, a formulation referred to in this dissertation as hybrid. The results from the binder (referred to as Resin 45 or simply R45) combined with the results for the hybrid provided a basis for identifying suitable models for evaluating the results for the propellant as a particle composite. The typical composition of HTPB solid propellant consists of 12.8 w% R45, 0.9w% isophorone diisocyanate (IPDI), 0.3w% methyl aziridine (HX-752), 18.5w% Aluminum (Al) particles (fuel particles), and 67.5w% ammonium perchlorate (AP), which serves as the oxidizer. The particles play a significant role in the mechanical properties of the propellant. In a typical particle composite, the addition of particles increases Y_{stress} values while decreasing Y_{strain} values. In the case of the irradiated hybrid and propellant specimens, the particles affect the stopping power and the electron range in the propellant. However, when propellant is irradiated, particle debonding occurs giving rise to particle to particle interaction, friction between particles and fracturing of the ammonium

perchlorate. The addition of the IPDI and the HX-752 serves several important functions leading to the creation of crosslinks in the propellant. By creating a network of connections between polymer chains in all directions within the matrix, the propellant achieves stronger properties that enable it to suspend the fuel – oxidizer particles, enable manufacturers to better handle the material and provide it greater material stability and resistance to mechanical failure.

1.4 Background

The analyses of the findings from the Galileo spacecraft in the mid-1990's gave rise to preliminary mission studies for further investigation of Jupiter's moon Europa. The concept for further investigation consists of an orbiter spacecraft capable of withstanding the radiation fields near and around Jupiter. Evaluation of mission concepts also explores the possibility of a Europa lander. This dissertation supports mission concepts to place a spacecraft in orbit around Jupiter (with the option of landing a rover) in order to perform a detailed investigation of the giant planet's moon using a highly capable, radiation-tolerant orbiting spacecraft with a lander. Similar to previous exploratory missions, the plan is to place the orbiter into a long, looping orbit around Jupiter to perform repeated close flybys of Europa prior to an attempted landing. However, risks to the mission are being investigated on account the Europa Braking Motor may be incapable of meeting its complete mission requirements after its solid propellant is exposed to the space radiation fields present in Jupiter's environment. It is necessary to investigate ionizing radiation effects in detail to establish greater confidence about the suitability of a commercially available HTPB solid propellant since it was originally not developed for a mission to Europa and the radiation fields can vary widely (Garrett, 1983).

Beginning with Pioneer 10 in 1972, seven missions have flown by Jupiter and two additional missions orbited the planet. These missions are the foundation for what is to be accomplished by a future Europa lander. The missions shown in **Table 1.1** have enabled mission planners to better understand the Europa mission requirements and anticipate the demands of the mission from Jupiter's particle radiation environment.

Table 1.1: Missions to Jupiter (Williams, 2017)

Mission (Sponsor)	**Mission Dates**	**Characteristics & Importance to Europa**
Pioneer 10 (NASA)	Launched: Mar 02, 1972 Arrived: Dec 03, 1973	Flyby: Provided images of Jupiter; measured radiation levels and magnetic fields **Importance**: Provided details about the demands of operating and signaling spacecraft travelling through high radiation fields. This included working through instrumentation failures resulting from exposure to Jupiter's intense particle fields.
Pioneer 11 (NASA)	Launched: Apr 06, 1973 Arrived: Sep 01, 1979	Flyby: Provided images of Jupiter's Great Red Spot. **Importance**: The two course corrections using liquid propellant thrusters due to strong magnetic fields demonstrated the effectiveness of hydrazine. Problems with its micrometeoroid instrument provided further insight into radiation effects of electronics. Also, demonstrated the benefit of high velocity flybys as a way of reducing radiation exposure while orbiting Jupiter.
Voyager 1 (NASA)	Launched: Sep 05, 1977 Arrived: Nov 13, 1980	Flyby: Provided images of Jupiter's moons **Importance**: The failure of its photopolarimeter demonstrated the adverse effects of strong fields. Provided detailed images of Jupiter's moon Europa. The mission showed Io having extremely active volcanoes releasing particles into space.
Voyager 2 (NASA)	Launched: Aug 20, 1977 Arrived: Aug 26, 1981	Flyby: Provided additional detail of the Great Red Spot showing it is a storm. **Importance**: Confirmed Io's active volcanos and Europa as having an icy crust.
Galileo (ESA/NASA)	Launched: Oct 18, 1989 Arrived: Dec 7, 1995	Orbiter/Probe: Orbited Europa providing detailed images of its red lines and red regions. **Importance**: Showed Europa's icy surface is still moving and forming due to thermal activity originating near the core of the moon.
Ulysses (NASA)	Launched: Oct 06, 1990 Arrived: Feb 04, 1992	Flyby/gravity assist: Performed a gravity assist maneuver at Jupiter to hurl itself out of the elliptic plane and into its solar polar orbit. **Importance**: Measured solar wind, interstellar dust and the three-dimensional character of solar radiation. Of particular importance is that this mission captured significant data about Jupiter's magnetosphere in relation to charged particle fields.
Cassini (European Space Agency (ESA)/NASA)	Launched: Oct 15, 1997 Arrived: Dec 12, 2000	Flyby: While its primary mission was Saturn, it analyzed the content of the Asteroid belt. Endured failure of its Plasma Spectrometer and Ultra Stable Oscillator. **Importance**: measured the three-dimensional structure and dynamic behavior of Jupiter's magnetosphere providing further evidence of the intensity of particle radiation fields.
New Horizons (NASA)	Launched: Jan 19, 2006 Arrived: Feb 28, 2007	Flyby/gravity assist: Primary mission to Pluto. Conducted measurements of Io's volcanic emissions. **Importance**: Jupiter flyby provided measurements of Jupiter's particle atmosphere, particle emissions from Io and the behavior of charged particles in the magnetosphere.
Juno (NASA)	Launched: Aug 05, 2011 Arrived: Jul 05, 2016	Orbiter: Measure Jupiter's composition, gravity field, magnetic field, and polar magnetosphere. **Importance**: Juno's cycle of perijoves demonstrated how to collect data while limiting the time inside intense radiation fields which can adversely affect electronics.

The combined knowledge from the former missions to Jupiter and its moons indicate that the radiation environments could affect the operation of the spacecraft and limit the performance of any onboard system if it is not, in some manner, protected from the intense radiation fields that are present. The Europa mission has a planned launch after 2025, will carry nine instruments, as shown in **Table 1.2**, and require about 5-years travel time to get to Europa in a flyby maneuver.

Table 1.2: Europa Mission Instruments (Foust 2015)

Instrument	Purpose
Plasma Instrument for Magnetic Sounding (PIMS): Johns Hopkins University (JHU), Advanced Physics Lab (APL), Laurel, MD	In the Jovian magnetospheric plasma PIMS will measure the density of flow velocity of ions with energies below 7 keV and the density and energy of electrons with energies below 2 keV. In Europa's ionosphere PIMS will measure the density and temperature of ions and electrons. By measuring magnetic perturbations in Europa's ionosphere, PIMS can also assist in searching for active water plumes and measuring their mass.
Interior Characterization of Europa using Magnetometry (ICEMAG): NASA Jet Propulsion Lab, CA	ICEMAG will use magnetic field sensors and helium sensors to measure electromagnetic waves between 0.01 and 1.0 Hertz in an effort to detect localized mass flow of ions originating from plumes and Europa's atmosphere.
Mapping Imaging Spectrometer for Europa (MISE): Jet Propulsion	The MISE instrument will be used to determine if Europa is capable of supporting life by searching and distinguishing between different types of amino acid signatures in the infrared spectra.
Europa Imaging System (EIS): Johns Hopkins University-Advanced Physics Lab	The EIS consists of a wide and narrow angle camera that will map most of the Europa moon at 50-meter resolution and capable of providing images of selected surface areas at up to 0.5-meter resolution.
Radar for Europa Assessment and Sounding: Ocean to Near-surface (REASON): University of Texas, Austin	The REASON instrument uses a dual frequency radar emitting High Frequency (HF) signals at 9 MHz and Very High Frequency (VHF) at 60 MHz with concurrent shallow and deep sounding to detect pockets of water within the ice shell.
Europa Thermal Emission Imaging System (E-THEMIS): Arizona State University, Tempe, AZ	E-THEMIS is an instrument that will be used to obtain thermal infrared images in three spectral bands from 7 to 70 micro-meters during multiple times of day of Europa's thermal behavior. This information will assist NASA identify thermal anomalies on the surface of the moon.
Mass Spectrometer for Planetary Exploration / Europa (MASPEX): Southwest Research Institute, San Antonio, TX	MASPEX is a high-resolution, high-sensitivity mass spectrometer developed to withstand high ionizing radiation environments. Its high resolution will enable MASPEX accurate determination of methane, water, ammonia, carbon dioxide, carbon monoxide, molecular nitrogen, argon, krypton and xenon.
Ultraviolet Spectrograph / Europa (UVS): Southwest Research Institute	UVS is a sensitive imaging spectrograph capable of making observations in the ultraviolet spectral range to locate and characterize plumes erupting from the surface of Europa.
Surface Dust Mass Analyzer (SUDA): University of Colorado, Boulder	The SUDA instrument will be used to measure the composition of solid particles released from Europa's surface due to meteoroid bombardment. The instrument has been designed to also measure the properties of small, solid particles originating from inside the Europa moon.

What continues to prompt missions to Jupiter and its moons is a search for places in the solar system that can sustain life. Once there, the Europa mission is expected to spend between 2 to 3 years performing a detailed investigation of Europa to validate previous information suggesting the presence of an ocean of liquid water beneath its icy crust that could sustain conditions favorable to life. The Europa craft's instruments will help confirm observations from the Hubble Space Telescope that suggest the presence of water vapor or plumes. These plumes are believed to originate from a subsurface ocean. Studying the composition of these plumes will enable a better understanding of Europa's potential habitable environment without having to extensively drill through the moon's ice layer. The current plan for the Europa mission may include up to 45 flybys that will vary in altitude between 25 km and 2,735 km above the surface of the Europa moon before attempting a landing. Plans also include placing an ice penetrating radar on the lander for determining the thickness of Europa's icy surface and search for subsurface lakes believed to exist similar to those below Earth's Antarctic.

Chapter 2. Literature Survey

The literature survey that provides the foundation for this investigation and its evidence of originality is divided into two main parts. The first part of the literature survey corresponds to those topics related to radiation science and the effects of radiation exposure of materials that exhibit similar properties to solid propellant. The second part corresponds to those aspects of the work that are not necessarily dependent on the effects of ionizing radiation, rather correspond to the study of propellant as a high particle composite material. This literature survey augments recent efforts on Europa Lander material selection considerations (Tappan & Heller, 2017) that focused on the ignition and burn propagation of the propellant While Tappan's work advances the understanding of propellant burn characteristics it does not cover propellant radiation sensitivity.

2.1 Radiation Effects on Polymers

The nuclear effects section of the literature survey principally consists of previous published works on radiation physics, Jovian radiation, the effects of ionizing radiation on spacecraft components, the development of Jovian radiation models, the effects of ionizing radiation on polymers and rubbers, and publications on radiation exposure of solid propellants. This investigation focuses on the effect of electron bombardment in solid propellant because the current literature does not provide sufficient clarity in the area of material damage and this is of significant interest to the Europa program. Specifically, there has been renewed interest in investigating the effect of electron bombardment on ammonium perchlorate (Miloshevsky, et al., 2017) to further investigate the radiation sensitivity of ammonium perchlorate in the absence of mechanical forces. For purposes of this investigation, the effects of electron bombardment on the aluminum particles are not as significant because the atomic structure in metals has an abundance of free moving electrons. Removing an electron in an energetic collision or by ionization results in a short disruption of the bond lasting long enough for a free electron to replace it (Dawson, et al., 1993). These electrons, which are typically very mobile and not attached to any particular atom, move from one

atom to another due to atomic forces. Dawson's work is important because electron bombardment will have a minor effect on the aluminum particles. The matrix, however, whose polymer structure consists of covalent bonds is characterized by the sharing of electron pairs. During electron bombardment, energetic electrons strip the electrons from the atoms in the matrix effectively breaking up the electron pairs in a bond. Energetic electrons break up the original molecules and create new and different molecules resulting in chemical change. The bulk of the investigations about irradiation of polymers and its effects on chemical structure show that when polymers are exposed to ionizing radiation, even at low doses, they experience structural changes coupled with molecular cross-linking, grafting and chain scission reactions (Ziaie, et al., 2005). Chain branching and crosslinking increase the molecular weight of a polymer, where crosslinking also forms an insoluble three-dimensional polymer network. Whereas, degradation or scission causes a reduction in molecular weight (Spadaro, et al., 2017). Respective of the ammonium perchlorate, molecular changes in polymers caused by ionizing radiation are the result of a combination of reactions that typically follow two processes when polymers are subjected to charged particle radiation (Al-Haik, et al., 2007). The first is charge absorption and the second is cleavage resulting from chain scission. The combined effects give rise to the formation of radicals, radical recombination that form cross-links, chain scission and gas evolution. These findings are important to this investigation because they elucidate the complexity of electron interactions in the propellant.

Electron transport in solids is inherently complex and has been the subject of investigations into the physical and chemical aspects of elastic and inelastic events that occur as electrons travel through a material. When bombarding electrons pass near neutral molecules, the electrons may transfer sufficient energy to remove outer shell electrons, producing additional free electrons and positive (molecular) ions (Kitson, et al., 1996). Kitson's work forms the basis for important efforts that improve probabilistic methods for modeling electron interactions that include electron total cross sections for the ionization and excitation of atoms and molecules by electron impact. To that end,

the National Institute of Standards (NIST) began developing and releasing the Elastic-Electron Scattering Cross Section Database in 1996 (Jablonski, et al., 2010). The work by the NIST, which continues to the day, provides a framework for investigation into the effects of electron interactions in different materials including trans-butadiene (C_4H_6) and serves to provide theoretical studies into elastic and inelastic behavior of polymers (Pandya, et al., 2011).

The fundamentals of electron impact ionization rely on ionization efficiency, commonly referred to as the yield, and the cross section (Gross, 2004). The work by Gross affirms that electron impact ionization produces positive ions by knocking a valence electron from the molecule of the material in question. As the electron passes near the proximity of a molecule the negative charge of the electron repels and alters the electron cloud surrounding the molecule. This interaction transfers kinetic energy from a fast-moving electron to the electron cloud surrounding the molecule. If sufficient energy is transferred in the process, the molecule will eject a valence electron and form a radical cation. Developments in expanding the understanding of analytical, empirical and classical methods for electron impact ionization continue to be the subject of more recent investigation (Haque, et al., 2016). Recent investigations by Haque take advantage of advancements in instrumentation and measurement to expand the understanding the physics of the collision process between electrons and different target materials.

Previous effort finds that Jupiter's magnetosphere is different to Earth's (Dessler, 1983). Dessler found that the energy required to drive the Jovian magnetosphere originates from the rotational energy of the planet rather than from the solar wind as is the case for Earth. Jupiter's moons behave like a plasma source that affect the structure and dynamics of Jupiter's radiation belts. Dessler describes Jupiter's magnetosphere as having three major regions that consist of (1) the inner magnetosphere; (2) the middle magnetosphere; and (3) the outer magnetosphere. Recent studies point to a new understanding of the Europa atmosphere and limits on geophysical activity (Shemansky, et al., 2014). Shemansky showed that a substantial fraction of the plasma species at the

Europa orbit are long-lived sulfur ions originating at Io, with approximately 25% of these ions originating from Europa. Investigations into the strength of Jupiter's magnetosphere reveal that Jupiter's dynamo generates the most intense planetary magnetic field in the solar system with a dipole moment of ~20,000 times greater than that of Earth and surface field magnitudes that are ~20 times greater than Earth's (Connerney, et al., 2017). The work by Connerney elucidates the origin of what gives energetic particles in Jupiter's system such high potentials. Related studies point to the possibility of active cryo-volcanism on Europa (Sparks, et al., 2017). In this work, the possibility of a repeating active source of erupting material on Europa is presented based on nighttime thermal images from the Galileo spacecraft. The images from Galileo provide different perspectives about thermal activity beneath Europa's icy surface.

Early studies into Jupiter's ultra-high frequency (UHF) radio emissions explain the magnetosphere in terms of trapped energetic electrons (Drake, et al., 1959). Drake's work provides the foundation for how energetic particles, namely electrons and protons, can affect the performance of spacecraft when exploring Jupiter and its moons. Further investigations (Rogers, 1995) report that the highest concentration of energetic particles in the magnetosphere is the Io torus that is situated between 5.5 – 8 radii of Jupiter (R_J). This is important for the planning of flybys of Europa prior to attempting a landing. The Ulysses spacecraft recorded measurements and images showing disc type distribution of protons inside the 17 R_J regime. Further analysis of Ulysses mission data (Anglin, et al., 1997) reveals that the equatorial proton flux decreases approximately exponentially with magnetic equatorial distance and is (approximately) linearly symmetric. As for the trapped proton population in Jupiter's magnetosphere, measurements from the Energetic Particle Detector used in the Galileo mission show that the population and energy profile for the protons are higher compared to that of other energetic ions inside the 20 to 25 R_J region (Mauk, et al., 2004). This work shows that beyond the trapped protons, Jupiter's strong magnetic field traps and holds very fast-moving electrons. Investigations into the shape of Jupiter's electron belts

(Bourdarie & Sicard, 2004) show that the population of energetic electrons is limited by absorption from Jupiter's moons and the Jovian ring rather by radiation loses. Investigation into optimum shielding methods for ionizing radiation in the Jovian environment affirm the most dominant particle constituent as high energy electrons with energies above 1 MeV (Cherng, et al., 2007). This is important because Cherng and his team assert that a significant amount of shielding is required to shield spacecraft electronics from the Jovian electrons, a finding that can be applied to all onboard systems including the propellant.

Previous work sponsored by NASA affirms findings by industry sectors on nuclear and space radiation effects on materials (NASA-SP-8053, 1970). Space radiation has been studied extensively respective of four sources consisting of (1) trapped belts; (2) galactic cosmic rays; (3) solar energetic events; and (4) solar wind (Normand, 2000). The work by Normand, in collaboration with Boeing Phantom Works, shows the trapped belts consisting of 10 keV to 5 MeV electrons and protons in the range of 100 keV to 500 MeV with the inner belt consisting of both electrons and protons and the outer belt consisting mainly of electrons. The vast majority of the published literature on space radiation effects has focused on the performance of electronics and thermal coatings, rather than propellant and motor performance. Work conducted at Johnson Space Center (FS-2002-10-080-JSC, 2002) highlights the complexity of space radiation in terms of the solar cycle and of the importance of investigating radiation effects as part of mission planning. Space radiation environments and related effects has been studied in terms of the relationships between primary and secondary effects (LaBel, 2004). This work, was the product of the Electronic Parts and Packaging Program at Goddard Space Flight Center. This Program continues to provide the framework for payloads and mission planning for space exploration with regard to how electronics behave in different radiation environments and achieve mission assurance by continually expanding the body of knowledge for missions like Europa.

An investigation into the interaction of nuclear radiation with plastic materials at low temperature revealed effects consisting of ionization; excitation; displacement of

the nucleus; scattering; and emission of secondary radiation (Evans & Morgan, 1982). Chemo rheology respective of radiation damage of elastomers was investigated (Ito, 1988) respective of the effects of chain scission and cross-linking on stress relaxation of a polymer. Electron bombardment induced crack initiation and crack growth in polymers and polymer surfaces has been investigated (Dickinson, 1988) with results showing acceleration of cracks from radiation exposure. In his investigations, Dickinson compared the results of stretched notched, polymeric materials before and after electron bombardment. For the unirradiated case, when a polymer sample is stretched, the notch opens into a wide crack tip, exposing a region of high stress concentration. However, when specimens where irradiated in a vacuum, electron induced crack growth occurred at stresses below the comparable stresses needed for crack growth of unirradiated material. The work by Dickinson attributes this behavior to high energy electrons interacting with the polymer through inelastic collisions. These inelastic collisions cause energy deposition in the material leading to vibrational excitations of the molecules, ionization, and broken bonds. In his work, Dickinson further explains that the chemical effects resulting from these interactions can be characterized into two principal effects corresponding to those that strengthen the material and those that weaken the material. The chemical effects resulting from electron bombardment that strengthen a polymer include polymerization, crosslinking or branching of the polymer. The chemical effects caused by electron bombardment that tend to weaken a polymer include bond scissions, molecular dissociation resulting from electronic excitations, electron-simulated desorption of ions and neutral species resulting from electronic excitations, or thermal degradation and gas evolution due to a temperature rise in the material being bombarded. Dickinson asserts that all of these events have mechanical consequences when a material is subjected to deformation.

Electron beam effects on polymers have been studied in relation to mechanical and thermal properties of electron beam-irradiated polyphenylene sulfide (Lopez, 1989). In his work, Lopez conducted and compared mechanical tests in both nitrogen and air environments. Mechanical tests carried out at 23 degrees C showed that

oxidative degradation occurs in air for high radiation doses. These results further show that modulus and tensile strength were not significantly affected by radiation level. For initially amorphous materials, the material became significantly brittle at doses above 1000 Mrad. Similarly, initially semi-crystalline materials became significantly brittle above 500 Mrad. Lopez used differential scanning calorimetry measurements to determine crystallinity and melting behavior to show the likely occurrence of crosslinking with high irradiation levels. This work also employed scanning electron microscopy to show the possible occurrence of gas evolution at the high dose levels.

The influence of electron beam irradiation on the chemical and structural properties of polyurethane has been extensively studied in relation to medical industry applications (Shin & Lee, 2013). The work by Shin and Lee showed that while polyurethane derivatives provide excellent flexibility and overall good irradiation resistance, high radiation doses alter the structure and function of macromolecules resulting in oxidation, chain scission and cross-linking. The results by Shin and Lee enabled the study of radiation crosslinking of polyurethanes (Ghobashy & Abdeen, 2016). In their work, Ghobashy and Abdeen explain how polyurethanes are produced by reacting an isocyanate $(N=C=O)_n$ with a polyol containing on average two or more hydroxyl groups per molecule $(OH)_n$. The aromatic isocyanates that include diphenylmethane diisocyanate or toluene diisocyanate (TDI) are more reactive than the aliphatic isocyanates like hexamethylene diisocyanate (HDI) or Isophorone diisocyanate (IPDI), which is used in HTPB propellant. Ghobashy and Abdeen found that while polyurethanes show higher radiation resistance compared with other polymers, the effect of ionizing radiation consisting primarily of chain scission, is highly dependent on the microstructure of the polymer, chemical composition, radiation environment and dose.

In the late eighties the effect of radiation cross-linking on the mechanical of polyethylene sheets using a Co-60 gamma source was investigated (Dongyuan, et al., 1987). Their work showed that the gel fraction of HDPE sheets increases with increasing dose and the average molecular weight of samples increased linearly pointing to

increases in cross-link density. Furthermore, Dongyuan's work showed that the mechanical properties inclusive of yield strength, breaking strength and breaking elongation percentage increased at low doses and then decreased at high doses further pointing to a change in dominant mechanisms, where cross-linking is dominant at low doses and chain scission at higher doses. The Young modulus of the samples in Dongyuan's work also increased linearly inside of the low dose regime.

Theoretical studies of radiation effects in composite materials for space use were investigated by NASA Langley (Chang & Kamaratos, 1982). The investigations by Chang contributed to defining the relationship between energy, range and stopping power elucidating the response of graphite fibers in epoxy from proton and electron radiation in the energy range between 0.01 and 10 MeV. The structural and chemical modification of polymer composite by proton irradiation has been studied (Shaha, et al., 2009) using a 3 MeV proton beam at a fluence of ~1000 ions/cm^2. In this work, the radiation induced changes in structural and chemical properties were studied by means of x-ray diffraction (XRD) and Fourier Transform Infra-red (FTIR) spectroscopy to show significant changes in morphology in irradiated materials pointing to off-gassing.

The effects of electron beam irradiation on mechanical properties of polypropylene (PP) / ethylene propylene diene monomer (EPDM) nanocomposites has been studied (Anuar, et al., 2011). The work by Anuar shows that while the tensile strength of specimens decreased with increasing clay particle content, the irradiated samples at 6 w% showed an increase before decreasing again. Anuar reports that this behavior is attributable to agglomeration of the particles and poor dispersion of the particles in the mixture. Anuar's work provides a basis for arguments for the enhancement in tensile strength attributable to dispersion and particle to matrix interaction with an optimum value for particle content. The effect of ion beam irradiation on metal particle doped polymer composites has been studied (Singh, et al., 2011). Singh reports that for polymethyl methacrylate (PMMA) with Ni powder additive, ion bombardment leads to converting polymer structure into a hydrogen

depleted carbon network. Singh attributes this to rupture of polymeric bonds resulting in the emission of hydrogen.

The effect of electron beam irradiation on the mechanical properties of acrylonitrile butadiene rubber with clay additives was investigated showing improvement in tensile strength and a reduction in strain values (Youssef, et al., 2015). Further studies into the use of gamma irradiation in preparation of polybutadiene rubber nano-powder were conducted (Abadchi & Jalali-Arani, 2013) respective of the effect on particle size, morphology and crosslink structure of the powder. These investigations showed that increasing radiation dose led to a decrease in C=C double bands corresponding to chain scission. Very recent investigations into the effect of electron bombardment on polyimide film continues to show that the interaction of high energy electrons with spacecraft materials leads to physical degradation of materials prompting the need to investigate radiation effects on propellant (Engelhart, et al., 2018).

The effect of ammonium perchlorate and associated decomposition from exposure to Co-60 gamma radiation was investigated in the mid 1960's (Radiation Applications Incorporated – RAI, 1965) under the guidance of the (US) Air Force Office of Scientific Research. The focus of this early investigation by the Office of Scientific Research involved the determination of the effect of gamma radiation on the deflagration rate of ammonium perchlorate oxidizer and independent of additives. The RAI study revealed that the irradiation of ammonium perchlorate by Co-60 gamma exposure resulted in the acceleration of burning rate for a particle size ranging between 150 to 210 micro-meters. When combined with 10% polystyrene, the burning rate of the ammonium perchlorate with polystyrene increased by approximately 10% after a dose of 100 Mrad. At 16% polystyrene the burning rate increased by approximately 13% after a dose of 100 Mrad. The combined findings of this early effort point to a relationship between radiation-induced cleavage and increased burn rate in a propellant.

The degree of crosslinking in polybutadiene caused by gamma radiation and the effect of microstructure and dose were investigated in the early nineties (O'Donnell & Whittaker, 1992). O'Donnell and Whitaker showed that crosslinking occurred in all three types of polybutadiene that were examined. Thermal decomposition of gamma irradiated ammonium perchlorate from low to very high radiation dose (above 100 Mrad) was investigated with the intent of assessing changes in intensity of NH_4^+ and ClO_4^- ions (Dedgaonkar & Sarwade, 1992). In this work, Dedgaonkar and Sarwade found that the loss of NH_4^+ stretching and bending frequency is much more rapid than the stretching and bending frequency of the ClO_4^-. These results point to NH_4^+ showing notable damage in the range of about 0.45 Mrad. The properties of HTPB based elastomers under the influence of gamma radiation were investigated (Dedgaonkar, 1993). These investigations focused on developing an understanding of the relationship and dependence between variable equivalence ratio NCO/OH and gamma dose. These efforts showed that with lower NCO content the ultimate stress increased with gamma dose and the ultimate strain decreased. These observations also included the occurrence of crosslinking and the formation of urethane. Dedgaonkar concluded in 1993 that stress-strain properties were affected by the presence of additives in small fractions. The study into diol-diisocyanate polymerization by gamma radiation also provided insight into alternative ways of curing (Dedgaonkar, Navle & Shrotri, 1993). In these investigations a mixture of toluene diisocyanate (TDI) and HTPB oligomer were irradiated using a Co-60 gamma source. These efforts were followed by investigations into the radiation effects on aging behavior of oligobutadiene-base urethane polymer (Dedgaonkar, et al., 1996). These efforts from 1996 provided insight into how Cobalt-60 radiation affect the aging of oligomer binder systems. The work by Dedgaonkar and colleagues compared traditional thermal induced aging of propellant to gamma radiation induced aging. After two-years the Co-60 induced aging samples showed slightly better mechanical properties than samples cured by thermal process.

Gamma radiation induced crosslinking up to 15 Mrad (dose) at room temperature was investigated to determine if crosslinking would lead to improvement

in the thermal stability of polyurethane samples (Ghobashy, et al., 2016). Similar in process to solid propellant, polyurethanes are produced by reacting isocyanate with a polyol having on average two or more hydroxyl groups per molecule $(OH)_n$. The work by Ghobashy shows that with increasing gamma radiation dose there is a corresponding increase in the crosslinking of the polyurethane samples. The work by Ghobashy further suggests that 5 Mrad is the upper dose for achieving benefit from radiation crosslinking. More recently and as a companion effort to this dissertation the radiation induced effects from electron bombardment of ammonium perchlorate in the absence of mechanical forces was investigated at NASA Marshall (Miloshevsky, et al., 2017).

2.2 Physical Behavior of Elastomers

The first of the hyper-elastic models was proposed by Mooney (1940) and later expressed in terms of invariants by Rivlin (1948). Since then, there have been several models developed with the intent of representing the behavior of unfilled, vulcanized elastomers. The following sections focus on the literature search of topics that are not directed related to radiation effects. These topics were found to be relevant because they relate or affect propellant performance in circumstances that are not necessarily related to a radiation environment. Work to investigate hyper elastic behavior of solid rocket propellant has received considerable attention in an effort to develop a library of propellant properties for solid propellants (Beyer & Graham, 1995). The work by Beyer and Graham significantly advanced the understanding of uniaxial stress vs strain relationships of highly filled HTPB solid propellant. Recent studies into fuel binder composition continue to focus on tensile strength and elongation measurements to model various types of stresses experienced during handling and transportation, thermal cycling, sudden pressurization on ignition and acceleration loads during flight (Mahanta & Pathak, 2012).

Relatively recent investigations by Merlette & Pagnacco (2012) into the structural dynamics of solid propellants with frequency dependent mechanical properties have served to further elucidate complexities in modeling polymer networks consisting of long polymer chains that are crosslinked to one another to form a network

of connections resembling a large, three-dimensional molecule. Merlette's work shows that rubber type solid propellants have polymer networks enabling them to have high elasticity. It is this high elasticity, which is attributable to a network of ideal chains that in part gives polymers like HTPB propellant their rubber-like behavior.

The early studies on solid propellant received considerable attention with regards to the relationship between processability and tensile properties and how this relationship manifested itself in crack propagation tests (Allan, et al., 1972). The work by Allan showed that molecular weight had negligible effect on HTPB propellant tensile behavior. The mechanism of the oxidative degradation of binder during the aging of composite solid propellant in the presence of polymeric binder and inorganic oxidant has been studied (Kishore, et al., 1979). Kishore's work shows that the presence of oxygen during aging significantly affects the mechanical properties of the propellant.

Significant effort to consolidate the body of knowledge for solid propellant chemistry took place in the 1990's under the guidance of the Indian Ministry of Defense (Kishore & Sridhara, 1999). The work by Kishore points to the importance of controlling process steps in preparing propellant as these will affect its mechanical properties. Studies into the thermal degradation of polyurethane propellant binder, namely HTPB, also took place at Sandia National Lab (Assink, et al., 1999). The work by Assink and team members concluded that crosslinking is the dominant process at higher temperatures and that degradation as a result of aging results in hardening of the material.

The influence of aluminum particle size on ignition and combustion of HTPB solid propellant containing ammonium perchlorate has been studied in order to characterize its combustion behavior (Olivani, et al., 2002). Olivani showed that the ratio of coarse to fine particles is an important consideration affecting the combustion of the propellant. The effects of particle size respective of particle to matrix adhesion were investigated to determine the effects of particle loading on mechanical strength properties of particulate in polymer composites (Fu, et al., 2008). Fu's investigations showed that particle to matrix adhesion and particle loading in polymers have a

significant effect on the mechanical properties of a particle composite. The mechanical characterization of composite solid rocket propellant using an HTPB base continued to be the subject of study and investigation (Gligorijevic, et al., 2015). The work by Gligorijevic shows how mechanical loads affect the reliability of the propellant.

The theory of rubber elasticity was the subject of considerable investigation in the 1930's (Kuhn, 1934). Kuhn developed the entropy model of rubber in 1934 providing the foundation for the understanding of polymer networks possessing hyper-elastic properties. In his work, Kuhn observed that in a stretched condition, rubber specimens become relatively stiff and lose their ability to oscillate. Kuhn's theory asserts that the relaxation of a stretched rubber specimen results in an increase in entropy and the transition of thermal energy into kinetic energy. Kuhn's investigations led to further explanation of the entropic origin of the elastic force (Guth & Mark, 1934). The work by Guth and Mark affirmed that the elastic force in Kuhn's model is proportional to the temperature of the specimen. This led to the assertion that the molecule is a dynamic system and that the number of polymer arrangements decreases once the rubber specimen is deformed. Kuhn's theory led to the development of Gaussian and non-Gaussian models for freely-jointed chains (Kuhn & Guth, 1943), (James & Guth, 1943). James & Guth in their work demonstrated that the shape and form of a material is controlled by the intermolecular bonds that link the molecules into a network. These investigations led to the further understanding that it is the number of bonds and their corresponding form of the material through their entropy instead of their internal energy that differentiates rubbery materials from solids. Interest in the development of models for elastic and highly elastic materials led to further investigation on worm-like chains (Kratky & Porod, 1943). Work on Freely Jointed Chain and Worm-Like Chain models provided the foundation for the study of the deformation and swelling of polymer networks with long chains (Hermans, 1946). Work on the study of deformation led to a fortuitous investigation of the relationship between polymer structure and mechanical properties (Stein & Tobolsky, 1948). Further elaboration on the statistical theory of rubber-like elasticity (Sakai & Isihara, 1948) revealed the

limitations of theoretical work of that period on the Gaussian distribution of polymer chains and the assumptions that the junctions of the polymer network are fixed.

The study of cyclic loading conditions with small strain amplitudes for rubber compounds was the topic of great interest in the early fifties (Fletcher, 1953). Continuing into the early sixties, investigations expanded into the effects of fillers, assessment of methods for accelerated aging and its effect on failure of rubbers (Payne, 1962). Continued efforts have included methods using both temperature and in limited instances, exposure to ionizing radiation with a focus in understanding material behavior in commercial nuclear (reactor) environments (Masayuki, 2007). In the decades that followed the work by Payne, further investigations affirmed the importance of the theory of rubber elasticity, as it relates to polymer science (Pearce, et al., 1977), demonstrating that the molecular theory of rubber elasticity is the foundation for investigating very large deformations followed by complete recovery (Flory, 1985). Drawing on advancements in the understanding of polymers sustaining large deformations investigators turned their attention to refining worm-like chain models (Bustamante, et al., 1994), and developing novel approaches for Extensible Worm-Like Chain models (Odijk, 1995) and Extensible Freely-Jointed Chain models (Smith, et al., 1996). In a study of statistical thermodynamics of rubber elasticity, the basic historical concepts and procedures advanced by Flory were further evaluated and explained (James, 2004). The work by James shows how in a real material the network of chains is more adequately resembled as an entanglement. More recently, in works related to properties and applications of polymer chemistry (Calhoun & Peacock, 2006) the relevant concepts are summarized in relation to two principal types of bonds. These include (1) chemical bonds which are represented by crosslinks between molecules and consist of covalent and ionic bonds; and (2) physical bonds, which are characterized by van der Waals forces.

Crosslinking is the process by which polymer chains are joined to form a three-dimensional network (Drobny, 2012). The work by Drobny points to the importance of crosslinking as a principal reaction to ionizing radiation. Studies into the mechanics and

chemistry of solid propellants respective of binder chemistry (Klager & Wrightson, 1967) showed that the mechanical behavior of the propellant depends on the number of crosslinks and the number of dangling chains in the binder and its interaction with its particle additives. The investigations by Klager and Wrightson indicate that failure in strained solid composite propellants starts in the binder by the formation of voids that propagate to the particles. It was also found that the bonding agent increases the modulus of the binder in the immediate vicinity of the particles. Increasing the modulus effectively delays the propagation of voids which ultimately leads to a debonding of the particles and irrecoverable loss of mechanical properties.

In polymers made up of -[CH_2 – CH_2]$_n$- structures, crosslinking is typically the dominant effect from radiation exposure, whereas, polymers having a tetra substituted carbon structure, chain scission tends to be the dominant effect (Kornacka, 2017). The work by Kornacka affirms the relationship between polymer structure and radiation effect respective of chain scission and crosslinking as shown in **Figure 2.4**.

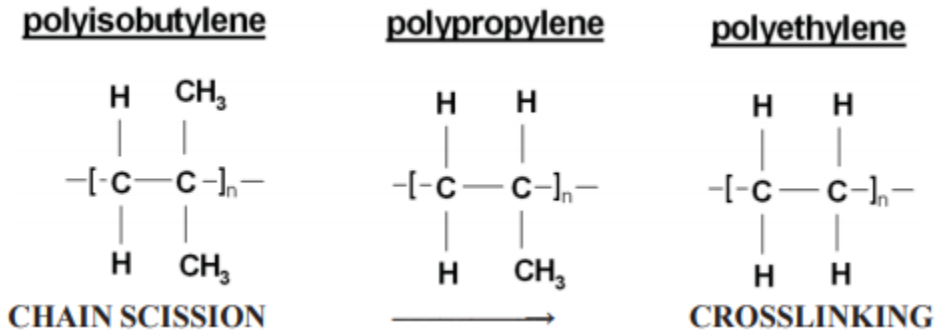

Figure 2.4: Ionizing Radiation Effects on Polymers (Kornacka, 2017)

The effect of electron irradiation on polytetrafluoroethylene provides relevant insight into the electron induced chain scission in a polymer (Mishra, et al., 2003). In this work, the resulting chain scission observed using FTIR spectroscopy was characterized by the formation of relatively stable free radicals, a decrease in melting point, reduction in thermal stability and a decrease in crystallinity of the polymer. The study of chain scission has been closely related to the study of electron beam curing of elastomers (Bhowmick & Vijayabaskar, 2006). The work by Bhowmick shows that the

irradiation of polymers results in grafting and crosslinking. Mechanical studies of electron induced degradation of poly (methyl methacrylate) and Kapton polyimide mark continued effort to explore the interaction between energetic electrons and polymers (Ennis & Kaiser, 2010). Ennis shows that electron induced degradation of polymers can vary significantly as a function of temperature. More recent investigations into changes in structural and thermal properties of Lexan polycarbonate were carried out using 8 MeV electrons (Hareesh & Sanjeev, 2011). In this work, Hareesh's found that radiation induced chain scission reduced crystallinity and crystallite size.

Long-chain branching is the process by which polymer chains are joined without forming a complete network of chains. The effect of long chain branching has been studied on rheological properties of polyethylene (Yan, et al., 1999). In his work, Yan investigated material properties to show that they are influenced not only by molecular weight and molecular weight distribution but also by long chain branching. Specifically, the chain structure has interactive effects that characterize a polymer's properties. Improvements in processability of polyethylene by radiation induced long chain branching using electron beam in ambient conditions have been investigated (Cheng, et al., 2009). Cheng and his team demonstrated that at low radiation doses, long chain branching led to changes in rheological properties evident by strain hardening at high extensibility and sag resistance at low shear rate. New developments in high energy electron beam induced long chain branched polyolefins for low density non-crosslinked polyolefins have been reported (Phillips, 2017). In his work, Phillips reports high energy electron beam modification as a means of improving the melt strength of commercially available Low-density Polyethylene (LDPE), High-density Polyethylene (HDPE) and Polypropylene.

Grafting is a reaction characterized by polymerization of a new monomer and attachment of the new chains to the main chain of the base polymer to effectively create a comb like chain. When high energy electrons interact with a polymer structure the resulting species can undergo further reactions that yield free radicals. These free radicals are the product of random interactions that in one instance they can recombine

to cause the polymer network to crosslink and in another they can react with monomers to initiate graft polymerization. Crosslinking is characterized by connections of polymer chains to create a network of connections whereas grafted polymers resemble a series of loose polymer strings connected to a central backbone, similar to a comb. Studies into this process have been investigated alongside crosslinking as mechanisms that enhance material characteristics (Chapiro, 1962). Investigation into the mechanisms affecting grafting and branching of comb-polymer structure focused on characterization of the molecular structure (Rempp & Franta, 1971). Improvement of polymer properties through the use of ionizing radiation has been investigated respective of the combined effects of grafting and crosslinking (Ranogajec, et al., 2009). Radiation induced graft polymerization has been investigated as a method for positively modifying surface and bulk properties of polymeric materials (Sanli & Gursel, 2008). Ionization and excitation interactions between electron beams and polymer structures continue to be investigated in relation to polymer species that react to yield free radicals (Lapin, 2014).

Investigations into particle composites demonstrated that adding particles to a polymer can increase the number of chains in the host, effectively distributing the load of a broken polymer chain (Fleminert & Bueche, 1957). Initial studies into the effect of oxidizer particle size on solid-propellant combustion stability were conducted at NASA Lewis Research Center (Morrell & Pinns, 1965). Morrell's investigation provided insight into the relationship between rate of combustion and the size of particle additives in the micrometer range. Further studies into optimum particle size and concentration also demonstrated that propellant burn rate is affected by the chemical properties of the contact surface between particles and matrix, and surface porosity (Hepburn, 1984). Investigations into particle size dependence of the Young's modulus of filled polymers (Vollenberg, et al., 1989) revealed that Young's modulus of a polymer is highly dependent on particle size. Investigation into the nonlinear viscoelastic behavior exhibited by solid propellant has led to advances in constitutive modeling to account for large deformation, debonding and cyclic loading effects as main sources of non-linear behavior of solid propellant (Jung, et al., 2000). Recent efforts in constitutive modeling

of solid propellant have led to greater understanding of particle debonding and the behavior of crack-tip damage respective of the mechanical behavior of a typical tensile specimen (Xu, et al., 2008). The work by Xu suggests that crack initiation occurs at the interface between the host and a particle. Of significance to this investigation are efforts on cohesive modeling of the debonding process in particle composites (Inglis, et al., 2005). In their work, the Inglis team showed that the interface between particles and matrix, volume fraction, particle size, and particle to particle interaction are all important characteristics that affect the mechanical behavior of a particle composite. Further investigations into the influence of the reinforcing particle shape and interface strength showed that particle fracture occurs by two mechanisms consisting of interface debonding and particle cracking (Romanova, et al., 2009). Romanova explained the contribution of particle cracking to the failure mechanism of a specimen. Investigation into mechanical properties of epoxy polymer with nano-silica particles (Zamaniana, et al., 2013) has shown that Young's modulus increased with the addition of particles. Investigations into the rheological and mechanical properties of natural rubber compounds filled with carbonized palm kernel husk and carbon black confirm that the incorporation of fillers enhances tensile strength, modulus, tear strength, abrasion resistance, and stiffness (Egwaikhide, et al., 2013). The work led by Egwaikhide affirms the understanding that the effect of particle additives depends on a complex interaction of several filler related parameters. These include particle size, shape, dispersion, surface area, surface reactivity, structure of the filler and bonding quality between particles and matrix.

The culmination of significant advances in understanding the mechanics and chemistry of solid propellants during the fifties and sixties was a collection of papers presented in 1965 at the Fourth Symposium on Naval Structural Mechanics held in Lafayette, Indiana and later published (Eringen, et al., 1967). This important work was sponsored by the US Navy's Office of Naval Research (ONR), and discusses mathematical and physical theories underlying the behavior of solid propellants, early nonlinear and linear theories of viscoelasticity, binder chemistry and combustion. Under the guidance

of the Chemical Propulsion Information Agency, a compendium of historical information on advances related to solid propellant mechanical behavior was collected by the Johns Hopkins University – Applied Physics Lab (APL) and serves as the predominant manual used by both private and public sectors (Chemical Propulsion Information Agency-CPIA, 1988). The work by APL provides the foundational knowledge for propellant behavior using uniaxial tensile tests at constant strain rates and serves as the guide for the Joint Army Navy NASA Air Force Propulsion Committee and this dissertation. Investigations into microstructural damage and fracture processes in composite solid rocket propellant were undertaken at University of California, Berkeley (Bencher, et al., 1994). The work at Berkeley was conducted using inert propellant to investigate voids, void growth due to crack propagation and particle delamination as a function of temperature. These investigations found that at the higher temperatures the weaker polymer matrix exhibited tearing more readily than at the lower temperatures leading to advancing the crack before particle delamination occurred. The effects of strain-rate and aging respective of temperature on the advancement of cracks in solid propellant were investigated (Ide, et al., 1999). These investigations revealed that lowering the temperature (from 60 to -40 deg. C) led to stiffening of the propellant resulting in decreased crack velocity. The microstructure and deformation mechanisms of solid propellant have been studied using 1H Nuclear Magnetic Resonance (NMR) spectrometry to investigate the spin – spin relaxation time (T2) as a way of measuring a highly-filled polymer's segmental mobility (Azoug, et al., 2015). Investigations of mechanical properties of irradiated polymers have been studied using tensile tests because these tests provide relevant information about the molecular modifications caused by ionizing radiation (Spadaro, et al., 2017).

Early investigations into mechanical properties of solid rocket propellant (Aerojet, 1961) showed the importance of debonding as a consideration in the mechanical properties of solid propellants. Investigations into the mechanical packing of spherical particles provided a framework for the behavior of particles suspended in binder (McGeary, 1961). These investigations were followed by efforts to characterize

the stress – strain function for highly filled elastomers (Farris, 1968). Farris showed that the uniaxial stress – strain behavior of highly filled elastomers is affected by voids in the material. These voids effectively reduce the rate at which the material accumulates mechanical energy giving rise to a material's stress-strain response. Efforts to model the complexity of mechanical failure of solid propellant respective of particle packing (Matous, et al., 2007) rely on modeling the progressive failure of particle to binder interface. Investigations into multiscale modeling of debonding damage in highly filled particulate composites continues to show particle debonding as one of the principal damage processes in solid propellants (Geubelle, et al., 2008). A recent compendium of advances in polymer composites respective of physical properties of macro and micro composites continues to show that mechanical properties of additive reinforced composites are dependent on the stability of the interfacial region between additive and host (Joseph, et al., 2012). Investigations into the influence of particle size distribution on random close packing of spheres followed the basic understanding that higher densities are achieved by using collections of particles of variable size (Desmond & Weeks, 2014). Efforts to model the effect of debonding continue to explore the relationship between interfacial debonding and propellant failure processes (Inglis, 2014). More recent investigations into the constitutive modeling of solid propellant damage due to viscoelastic debonding was conducted respective volumetric strain (Soo Yun, et al., 2016).

The mathematical approach for evaluating and modeling the effect of fillers on the properties of polymer composites depends on (1) particle concentration; (2) particle characteristics; and (3) particle interaction with the matrix. One of the earliest approaches for a system of suspended particles in an elastomer is based on Einstein's equation for the viscosity of suspended rigid spheres (Einstein, 1956). In the case of non-spherical particles, the orientation of the particles is also important in determining strength properties (Ahmed & Jones, 1990). Further review of the literature confirms that particle characteristics typically include their physical composition, particle

dimension, particle shape, homogeneity of distribution and adhesion level are relevant considerations in the evaluation of composite properties (Nielsen & Landel, 1994).

One of the earliest theories for an elastomer composite system is based on Einstein's equation for the viscosity of a suspension of rigid -spherical inclusions. However, Einstein's equation is constrained to low concentrations of particle additives because it does not account for the strain fields around particles or their interaction. The limitations associated with particle interactions led to further investigation and adaptation of the Einstein equation to account for particle crowding (Mooney, 1951) and was further articulated to account for non-spherical particle geometry (Brodnyan, 1959). The mathematical approach to account for non-spherical geometries in a polymer composite also considered the effect of different loading conditions on mechanical properties. These loading conditions typically consist of static tests, transient tests, impact tests, and cyclic tests. The most common of these is the static test consisting of standard tensile tests. Tensile tests are used throughout the literature to measure force response when a polymer is placed under strain at constant rate. Tensile tests have provided the ability to characterize the mechanical properties of a polymer in relation to strength, strain and modulus. An important detail reported in the literature is that a polymer can be made stiffer by incorporating rigid particles. In previous studies, the mechanical properties of a polymer are achieved when load transfer exists between the matrix and the particles that constitute the reinforcement for the composite (Hu, et al., 2003). Solution methods also rely on an understanding that the load transfer between matrix and reinforcements can be increased with the addition of chemical crosslinks (Valavala & Odegard, 2005). The methodology of present-day polymer mechanics is the product of several theories that have been advanced to explain and model the tensile modulus of non-interactive composite materials. Six of the more prominent theories over the last hundred years include the Einstein model; the Guth model; the Quemada approach (Quemada, 1977); the Kerner approach (Kerner, 1956), and the Sato and Furukawa (Sato & Furukawa, 1963). An important consideration in the mathematical treatise of elastomers is the determination

of cross-link density. In cases where it has not been possible to discretely evaluate materials, the crosslink density has been calculated from the degree of swelling of a material. Under the current investigation, the University of Idaho mold enabled for binder to be molded under controlled conditions to produce I-bone specimens effectively avoiding the need to swell composite specimens. The use of a mold to produce binder specimens does not require the cutting of material, which in turn provides dimensional accuracy in the specimens used for testing and computing crosslink density.

Chapter 3. Experimental Set-up

The following sections elucidate important aspects in the process of producing specimens. HTPB is composed of an oligomer of butadiene that is terminated at each end with a hydroxyl functional group. When combined with IPDI, these form polyurethane polymers. Polyurethane binders provide solid propellant grains with stable physical properties that in industrial applications enable them to be processed into unique shapes. It is common in the propellant industry to use hydroxy terminated polybutadienes as prepolymers for these binder systems. These prepolymers consist of a backbone of repeating polybutadiene units with hydroxyl sites that provide the necessary cross-linking for hardening the propellant. The time required for preparing a solid propellant grain is dependent on pot life, cure time and aging, which are typical of resins. Pot life in this instance is defined as the time required for the mix to reach a viscosity required by the manufacturer, and is typically in the range of one to several hours. The surrogate, hybrid and propellant materials used in this investigation were poured into block boxes sized to correspond with the JANNAF sample dimensions as shown in **Figure 3.1** (with dimensions in inches).

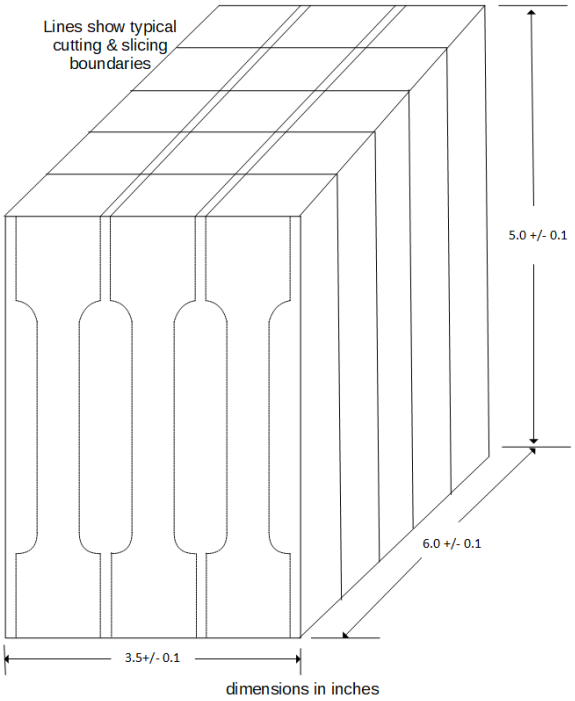

Figure 3.1: Typical JANNAF Cast (JANNAF-PC, 1988)

Once cured, a typical box can yield up to 15 specimens. However, the cutting process required to produce I-bone specimens, as denoted by the lines in Figure 3.1, often renders some specimens unusable due to variations in slicing or during die cutting. For the purposes of this dissertation, a single box would normally produce nine specimens suitable for testing. The boxes were cured at an elevated temperature for a period of several weeks and then aged for approximately 40 to 50 days. While the process of using boxes was applied successfully for surrogate, hybrid and propellant, block boxes proved to be impractical for the binder because it could not be easily cut. Instead, binder specimens required the use of a mold to eliminate the need for cutting.

3.1 Mixing, Curing & Aging

The mixing achieves a balance of fuel and oxidizer in the processing of a solid propellant. Specifically, the mixing process aims to provide sufficient oxidizer for the fuel particles to perform at optimum. During the mixing process for the materials used in this investigation, it was essential to ensure weights and measures were performed correctly to enable the isophorone diisocyanate (IPDI) to work well. Since the amount of solid particulate in the HTPB propellant is very high in solid content, nearing 89%, viscosity played a significant factor in the processing of the material. The addition of a catalyst was also important because when added to the diisocyanate curing agent it performs as a wetting agent effectively lowering the viscosity of the propellant to enable better mixing and contact with the particulates. The period after mixing, or pot life, was typically a few hours.

Curing began once all ingredients were mixed and poured into a box mold. Elevating the mixing and curing temperature lowers the viscosity of the propellant. However, elevating the temperature during mixing and curing results in stresses as the material cools down to 25^{o}C (77^{o}F). During the curing process it is necessary to maintain a constant temperature so that the particles do not expand and contract; this eliminates the possibility of creating voids in the material which could lead to poor test results. Therefore, special attention was given to eliminating voids during the specimens used for and explained in this dissertation. The time for curing the materials

used in producing specimens for this investigation was between 11 to 15 days. Both pot life and cure time are dependent primarily on the speed of the reaction between the hydroxyl terminals of the prepolymer and the polyisocyanates. While it was not exercised in this investigation, excessive pot life and cure time may be shortened by the use of urethane cure catalysts. Curing of the specimens was accomplished in a controlled setting at an average temperature of ~50^{o}C. This temperature was selected based on laboratory experience and protocol to avoid excessive strain in the cured grain caused by cool down to ambient temperature after processing. Normally temperatures can be elevated as high as 60^{o}C during curing with an upper limit of about 71^{o}C depending on familiarity with the material.

During aging the propellant undergoes changes that affect its strength and strain values. The aging process typically begins a day or two after the propellant has fully cured and removed from its curing environment. The effects of aging on HTPB propellant have been studied to indicate instabilities occurring within 40 days after curing (Gligorijevic, 2014). The results for Y_{stress} as a function of time are shown in **Figure 3.2**, and provide perspective as to how propellant properties continue to change well after its curing period. In an industrial application where the propellant will sit for extended periods the period immediately following the curing stage may not be that significant. However, in the case where propellant samples are to be prepared for testing, vigilance is required during the aging period to ensure consistency in results.

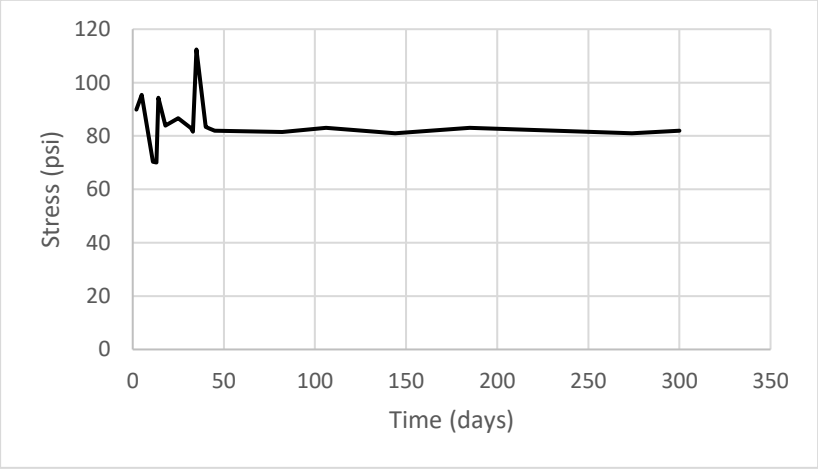

Figure 3.2: HTPB Stress vs Aging (Gligorijevic, 2014)

In relation to Y_{strain}, a similar behavior over the first 40 days of aging is seen in **Figure 3.3** suggesting that the propellant continues to cure.

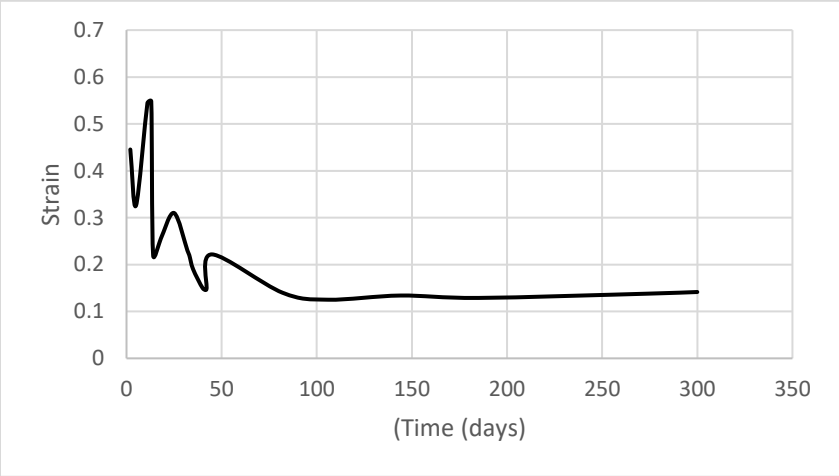

Figure 3.3: HTPB Strain vs Aging (Gligorijevic, 2014)

Reported values of HTPB propellant aging suggest that to obtain reasonably accurate Y_{stress} and Y_{strain} values it is important to age the material for 40 to 50 days before subjecting it to mechanical tests. During the aging period two principal mechanisms take place consisting of (1) oxidation of the propellant that in turn leads to chain degradation and (2) oxidation-induced crosslinking (Yang, 2017). The fluctuations in both Y_{stress} and Y_{strain} seen in **Figure 3.2** and **Figure 3.3** inside of the first 40 to 50 days suggest that mechanical testing prior to this period could lead to uncertainty in results.

The oxidation reactions that occur are responsible for the oxidation-induced crosslinking that characterizes the first 40 to 50 days after curing and results in the development of an entire network of chains. This network of chains makes the propellant stiff enabling it to harden and be handled, or in the case of this investigation, enable it to be die cut using standard cutting procedures for the JANNAF configuration. So, while there are two types of oxidation reactions taking place during aging, the oxidation-induced crosslinking eventually overtakes chain degradation (Yang, 2017). Overall, the change in mechanical properties of the propellant is due to oxidation-induced crosslinking.

3.2 Specimen Preparation

The test campaign was divided into two phases, the first was for the surrogate and the second was for the propellant. The aim of the surrogate phase was to develop an understanding of how ingredients affect the mechanical performance of the propellant. However, for the surrogate, ammonium sulfate was used instead of ammonium perchlorate because of the safety concerns and risk of explosion with ammonium perchlorate. With the exception of the ammonium sulfate that was used instead of the ammonium perchlorate, the surrogate mix consisted of the same ingredient proportions as HTPB propellant.

The propellant phase consisted of preparing specimens beginning with binder, then preparing specimens using binder and aluminum (hybrid) and progressing to evaluating propellant. All specimens were casted to Joint Army Navy NASA Air Force (JANNAF) I-bone dimensions. The binder was not casted, rather, it was molded due to the complexity of cutting the material. Typical representative dimensions for the JANNAF ½ inch I-bone sample are shown in **Figure 3.4** (with dimensions in inches).

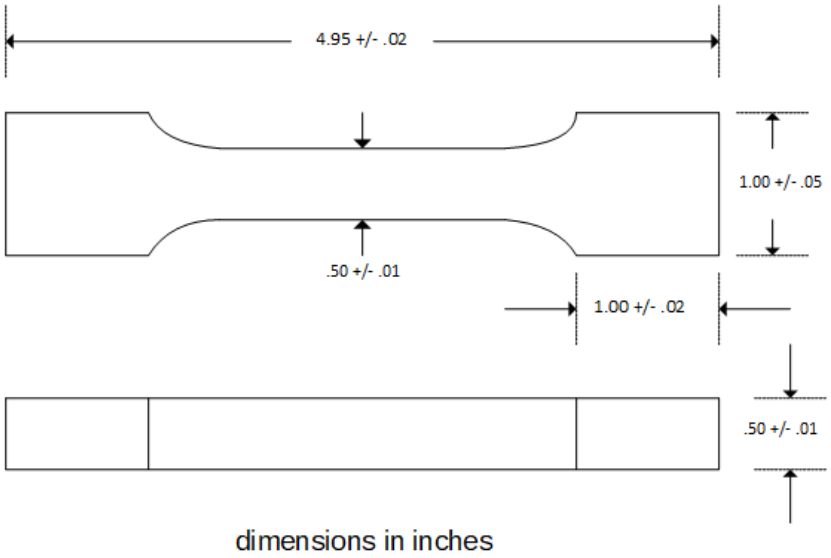

Figure 3.4: JANNAF Specimen (JANNAF-PC, 1988)

I-bone specimens were die cut from slices taken from the box stock once cured. A typical slice taken from a box is shown in **Figure 3.5**. The slice in **Figure 3.5** is that of

surrogate material where the outline of the I-bones is traced to facilitate the placement of the die-cutter. Each slice typically yields three I-bones.

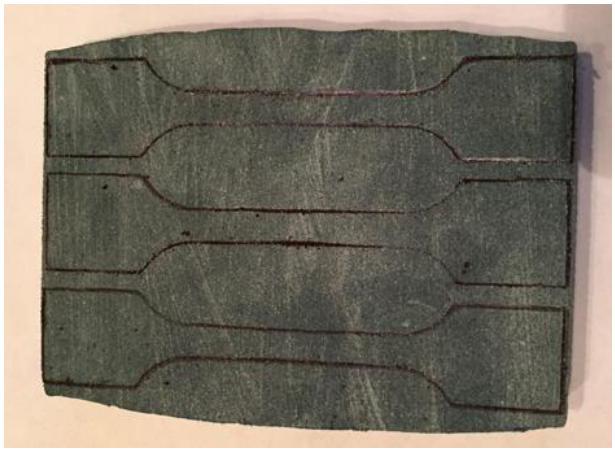

Figure 3.5: Slice of Surrogate Material

Once slices are marked for cutting with the outline of the I-bones, a die cutter is used for producing individual specimens. A typical die cutter used for creating I-bones is shown in **Figure 3.6**.

Figure 3.6: I-bone Specimen Cutting Die

While under ideal conditions each box of cured propellant may yield as many as 15 specimens, the cutting process often damages I-bones effectively reducing the yield from each box. The best nine specimens are then selected for testing. As mentioned previously, a mold was used for binder specimens and is shown in **Figure 3.7**.

Figure 3.7: Mold Used for Binder Specimens

The mold was fabricated at the University of Idaho and successfully used in preparing binder I-bone specimens for this investigation. The mold produces nine binder I-bones per batch with minimal waste of material. It was necessary to use a mold for the binder because the material cannot be readily cut using standard tools and devices. Binder specimens were prepared using the formulation of the propellant with the exception of the particle additives and consisted of HTPB-R45 resin (89.8w%), IPDI (10.19w%) and HX-752 (0.01w%). Preparing binder specimens in the JANNAF configuration presented significant challenges where the traditional casting and cutting methods proved unsuccessful. A typical unirradiated binder specimen created in the U of I mold is shown in **Figure 3.8**.

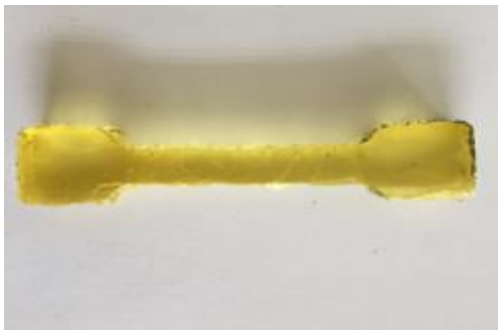

Figure 3.8: Typical Binder Specimen

The addition of aluminum particles changes the color of the binder dramatically from the amber – yellow color to a greyish metallic color as will be shown later.

3.3 Irradiation of Specimens

Prior to the irradiation of specimens, it was necessary to determine the penetration of electrons into each of the materials to be tested and the corresponding radiation dose. Before irradiating specimens, it was necessary to check the range of 2 MeV electrons in the binder, hybrid and propellant. This step was necessary to investigate the stopping power of the materials and range of the reference electrons with regards to the geometry of a typical JANNAF specimen and to determine if the 2 MeV electrons would have sufficient penetration. The Pelletron uses a single beam for irradiating samples, which required that at 2 MeV the specimens to be turned 180 degrees to be irradiated on both sides. A determination of the mass stopping power and corresponding range were performed using the National Institute of Standards (NIST) Electron Stopping Power & Range (ESTAR) model (Seltzer, 2016). The collision stopping power for different materials is calculated in ESTAR from the Bethe formula (Bethe, 1930 & 1932) with correction for density effect related to the ionization loss of charged particles travelling through a material (Sternheimer, 1952 & 1982). The stopping power formulation in ESTAR uses a mean excitation energy parameter that is referred to as the I-value which is representative of the stopping properties for different materials. I-values are normally determined experimentally relying on measurement of proton and alpha particle stopping powers and ranges in materials of different densities. The uncertainties of the calculated collision stopping powers for electrons in ESTAR were estimated by the International Commission on Radiation Units and Measurements (ICRU, 1984) to be 1 % to 2 % above 100 keV, 2 % to 3 % (in low-Z materials) and 5 % to 10 % (in high-Z materials) between 100 keV and 10 keV, which works well for the 2 MeV reference energy used in this dissertation. The uncertainties at low energies are due to the lack of corrections to account for the velocity of the incident electron no longer being sufficiently greater to the velocities of the atomic electrons. Because of this consideration at the lower energies, ESTAR stopping powers are usually restricted to energies above 10 keV. Consistent with the ESTAR model parameters, electron energies were evaluated in the range from 0.01 MeV to 2 MeV. The numerical results for mass

stopping power results (MeV * cm^2 / gm) for the three materials studied in the propellant phase are shown in **Table 3.1**.

Table 3.1: Numerical Results for Stopping Power Comparison

Electron Energy (MeV)	Binder (MeV cm^2/g)	Hybrid (MeV cm^2/g)	Propellant (MeV cm^2/g)
0.01	20.1	22.1	19.1
0.1	3.72	4.02	3.58
1.0	1.71	1.81	1.64
2.0	1.71	1.8	1.64

Numerical values for penetration (depth) in each of the three materials between 0.01 MeV to 2 Mev using ESTAR are shown in **Table 3.2**.

Table 3.2: Numerical Results for Penetration Depth

Electron Energy (MeV)	Binder (cm)	Hybrid (cm)	Propellant (cm)
0.01	6.5E-04	4.4E-04	2.9E-04
0.1	3.5E-02	2.4E-02	1.5E-02
1.0	0.77	0.54	0.34
2.0	1.5	1.1	0.67

Considering that the geometry of a typical JANNAF specimen requires a penetration depth of ~0.635 cm, the results show that 2 MeV electrons offer sufficient range to reach and irradiate the specimen through to its central axis. **Figure 3.9** shows a representation of the numerical results for penetration in the three materials studied.

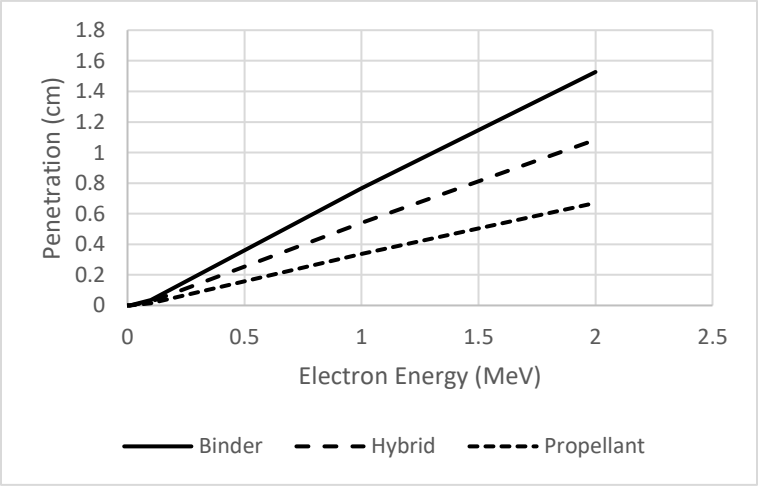

Figure 3.9: Numerical Results for Electron Penetration

Range calculations for the purpose of evaluating transport phenomena tend to be complex due to cascading effects. However, the ESTAR results provide insight into the relationship between particle energy and mass stopping power. The resulting reduction in range for electrons interacting in a high-content particle composite material is normally due to a combination of interactions that include ionization, Bremsstrahlung (where X-rays are created from electron deceleration), and elastic scattering from nuclear and electronic interactions. Of these, elastic scattering is likely to be a dominant effect (Hemmerich, 2000) in most polymers. A complete characterization of the path of electrons and their interactions is typically predicted using transport theory of which the Monte Carlo method is a practical technique especially when determining the corresponding dose of specimens in the Pelletron. The ESTAR model provides a comparison of nominal range for electrons of different energy undergoing multiple interactions in a material. However, to determine radiation dose to the specimens with greater accuracy, it is necessary to consider different interaction-mechanisms.

For dose calculations, a Monte Carlo solution (MONSOL) was used by MSFC for purposes of determining the necessary exposure and corresponding dose from the electron beam. MONSOL is a computational tool that employs the Monte Carlo technique to carryout numerical trials on the effects of high energy electrons, positrons, photons, ions and neutrons on three-dimensional composite materials (Miloshevsky, 2017). Specifically, MONSOL adapts the Monte Carlo technique to model electron-photon transport to incorporate a mixed scattering model for the simulation of charged particle transport in materials. MONSOL is capable of simulating electron interactions using a combination of approximations for close collisions and distant collisions within a broad band of predefined scattering angles and energy losses in a material. MONSOL is able to simulate close collisions in detail by combining available data from sampling methods with analytical differential cross sections for different interaction mechanisms that include the photoelectric effect, Compton scattering, and electron-positron pair production. Distant collisions are treated using multiple scattering theory where the simulation of photon transport is proportional to the mean number of interaction

events in a given trajectory. Previous efforts at MSFC to conduct dose calculations from electron and Bremsstrahlung penetration in the 1970's (Watts & Burrell, 1971) using the Berger Monte Carlo approach produced an effective method for electron transport using linear and continuous deceleration approximation. The work by Watts & Burrell at MSFC produced accurate dose calculations to within 3% of measurement in aluminum.

In order to predict a uniform dose to the optimum extent practical for specimens in the Pelletron, it was necessary to rely on Monte Carlo modelling performed by MSFC. The use of Monte Carlo technique enabled a more precise calculation of the dose considering radiation measurement in the target chamber of the Pelletron was not feasible. The Monte Carlo model MONSOL enabled MSFC to compute the dose to each side of the specimens. Monte Carlo technique accounts for primary and secondary interactions that occur between electrons and the specimen material with particular consideration to the dose attributed to Bremsstrahlung. **Table 3.3** shows a representative breakdown of the combined dose per specimen as a function of electron beam energy.

Table 3.3: Dose Details for the Irradiation of Specimens

Target Dose (rad)	Dose Fraction	Beam Energy (MeV)	Fluence (e/cm^2) per side
6.0E+06	77%	2.0	1.16E+14
	10%	1.0	1.50E+13
	13%	0.6	1.95E+13

The irradiation of specimens was conducted at the Pelletron Combined Environmental Effects Facility. A photograph of the radiation facility where the samples used in this dissertation were irradiated is shown in **Figure 3.10**. The EM41 Pelletron generates a one directional beam directed at a chamber sufficiently large to place several JANNAF I-bone specimens at a time.

Figure 3.10: EM41 Pelletron Accelerator

For the reference energy of 2 MeV electrons, the penetration depth into the specimens is insufficient to penetrate the entire thickness of the I-bone and achieve a uniform radiation dose profile across the thickness of the specimens so the I-bones had to be manually "flipped" to effectively irradiate them from both sides. **Figure 3.11** shows the configuration for the exposure of the I-bones in relation to the electron beam.

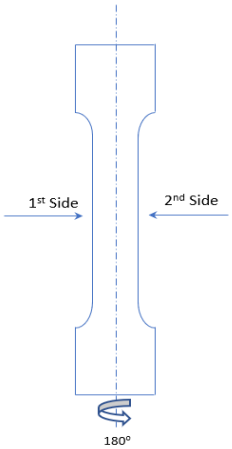

Figure 3.11: Typical Configuration of Specimens during Irradiation

Furthermore, to achieve a uniform dose across the thickness of each specimen set, a metallic screen, or filter, was used to achieve a uniform radiation dose across the

thickness of each specimen. The use of a metallic filter ensured that electrons that are sufficiently energetic to reach the center of the specimen pass to interact with the material. The beam was aimed to deliver the optimum radiation dose at the center of each specimen. The process of turning a specimen 90 degrees to achieve a dose on both sides leads to a higher dose at the center of a specimen as shown in **Figure 3.12**.

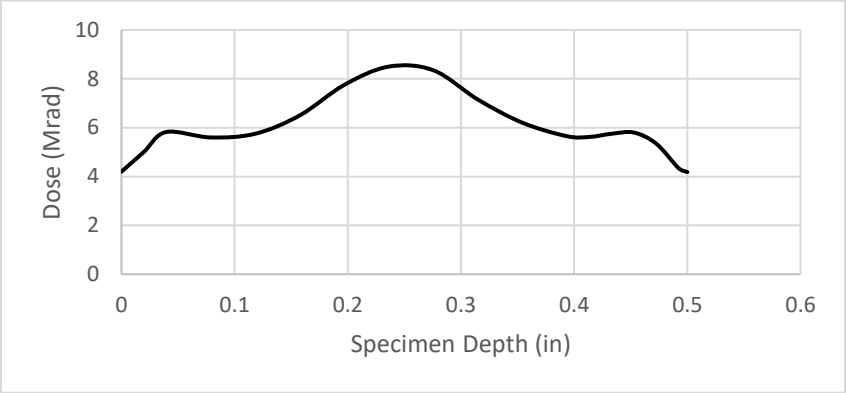

Figure 3.12: Typical Dose Profile (Unfiltered)

To compensate for this higher dose toward the center of the specimen, MSFC used a metallic filter (~1.2 mm aluminum) to attenuate the less energetic electrons and allow those electrons capable of reaching the center of the specimen. The dose profile achieved from using the filter is shown in **Figure 3.13.**

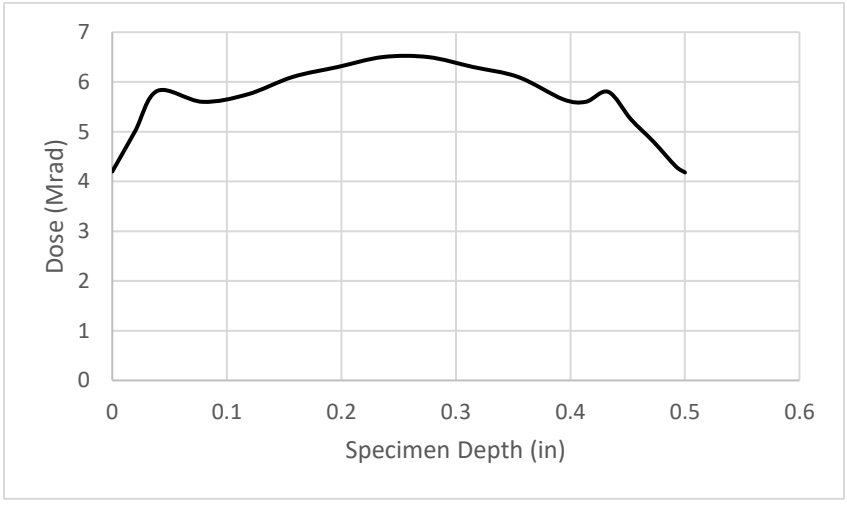

Figure 3.13: Typical Dose Profile (Filtered)

In looking at **Figure 3.13** it can be seen that the predicted dose deposited in the specimens is not exactly at 6 Mrad and a s a result the 6 Mrad is a reference dose. The Monte Carlo method used introduces error because it is based on transport theory as opposed to measured dose. MSFC performed validation of the MONSOL code used in these dose profiles and based on comparisons with trajectories in aluminum determined comparable results (Miloshevsky, 2017).

3.4 Mechanical Testing

Tensile tests were conducted using a Materials Test Systems (MTS) Insight (Model 43) 30 KN standard test machine as shown in **Figure 3.14**. The MTS Insight device utilizes the "TestWorks 4" software for tensile testing of JANNAF I-bone specimens. The 30 kN tensile capacity machine is outfitted with a special grip as shown on the right of the image in **Figure 3.14** enabling it to secure I-bone samples during standard pull tests.

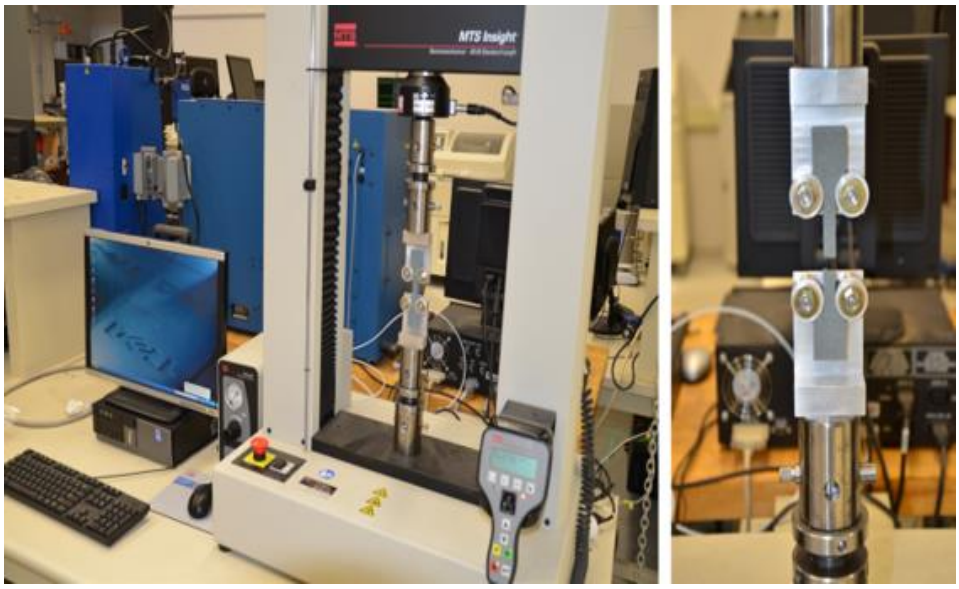

Figure 3.14: MTS Test Machine Pulling a JANNAF Specimen

Values for Maximum Extension, Y_{stress}, Y_{strain} and elastic modulus are computed directly from outputs of the MTS Model 43 system used in the mechanical (pull) tests at a strain setting of 2.0 inches/minute. The testing procedure of the Model 43 follows the

Chemical Propulsion Information Agency (CPIA) manual for Solid Propellant Mechanical Behavior (JANNAF-PC, 1988).

Chapter 4. Results

Similar to the manner in which specimens were prepared for testing by dividing them into a surrogate phase and a propellant phase, the results are presented in the same manner. The surrogate phase did not include pull testing of irradiated specimens. However, a small sample of surrogate was irradiated to determine the radiation dose at which the ammonium sulfate particles showed damage in the form of cleavage. Results for the unirradiated and irradiated binder, hybrid and propellant are provided in the sections below

4.1 Surrogate Phase Results

The surrogate phase consisted of preparing and testing unirradiated specimens of inert material where the ammonium perchlorate was substituted with ammonium sulfate (AS). The surrogate phase provided insight into three important areas. First, the results from tensile tests on unirradiated surrogate determined how changes in quantity of ingredients used in HTPB propellant affect Y_{stress} and Y_{strain} values. Second, the results from tensile tests provided a range of Y_{stress} and Y_{strain} values representative of different propellant mixes in order to support the development of models used in this dissertation. Third, a small section of surrogate material that was irradiated and imaged using SEM scans provided insight into the radiation dose at which the ammonium sulfate experienced cleavage. This comparison showed the AS experiencing cleavage at a higher radiation dose (32 Mrad) than ammonium perchlorate (5 to 16 Mrad).

The baseline formulation of the surrogate contained HTPB-R45 ~12.8w%, IPDI (isophorone diisocyanate) ~0.9w%, HX-752 (methyl aziridine) 0.3w%, aluminum (fuel) ~18.5w%, coarse ammonium sulfate (surrogate) ~47w% and fine ammonium sulfate ~20.5w%. The surrogate specimens were casted, cured, aged and cut. Tensile tests on surrogate specimens provided a range of Y_{stress} and Y_{strain} values for propellant from 115 psi (at 20% strain) to 173 psi (at 65% strain). This range of values provided important values for the models used in this dissertation. A baseline for the surrogate that is closely representative of the ingredients of the propellant was tested and the results of are shown in **Table 4.1**.

Table 4.1: Representative Tensile Test Results for Unirradiated Surrogate

Max Extension	0.6 in (+/- 0.02 in)
Y_{stress}	133.1 psi (+/- 4 psi)
Y_{strain}	22.4% (+/- 3%)

While the surrogate baseline results did not precisely mirror values for unirradiated propellant of Y_{stress} (115 psi) and Y_{strain} (43%), the results from surrogate do provide the necessary range to model the behavior of the propellant. The strain vs stress graph for the surrogate baseline is shown in **Figure 4.1**.

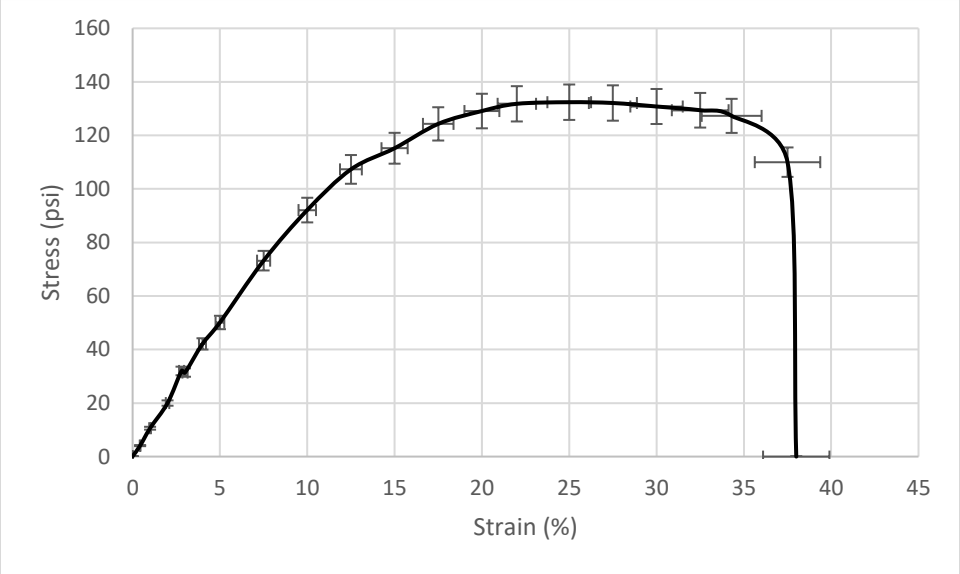

Figure 4.1: Stress – Strain Curve for Unirradiated Surrogate

The data collected from mechanical tests of surrogate specimens were evaluated using analysis of variance (ANOVA) to determine how the individual ingredients affect Y_{stress} and Y_{strain} based on the values recorded. One-way ANOVA was used to determine which ingredients have a significant contribution. Two-way ANOVA was used to confirm increases in key ingredients affecting Y_{stress} and Y_{strain}. The process consisted of grouping the results for Y_{stress} and Y_{strain} into three groups each corresponding to low, medium and high concentration for the principal ingredients used in the surrogate

samples. ANOVA was applied to the results of a Design of Experiment (DOE) to determine whether the means of three groups of surrogate propellant are different. The DOE consisted of twenty-seven sets of surrogate specimens. Each set consisted of nine specimens. The twenty-seven sets were divided into three groups of nine, with one group representing low content, a second group representing medium content and the third representing high content. With each group having nine sets, each group consisted of 81 specimens.

For the surrogate samples one-way ANOVA showed that increasing the quantity of IPDI and HX-752 from low concentration to medium concentration did not cause a significant change in Y_{stress}. However, increasing the concentration of IPDI from low to high (16% increase) in the binder did cause a detectable change in Y_{stress} as shown in **Table 4.2**. Doubling the concentration of HX-752 (low to high) also had a significant effect on propellant Y_{stress}. The concentration of IPDI and HX-752 was varied according to known formulations of HTPB propellant.

Table 4.2: One-way ANOVA Results for Surrogate Y_{stress}

Ingredient	F	P Value	Significant?
IPDI	3.51	0.04	Yes
HX752	4.03	0.04	Yes
Aluminum	0.16	0.85	No
Ammonium Sulfate (Coarse)	1.18	0.33	No
Ammonium Sulfate (Fine)	2.04	0.16	No

In evaluating these results, the significance of the ingredient is established when the 'P value' is less than 0.05. These results show that the quantity of HX-752 and IPDI in the mix is an important ingredient affecting Y_{stress} in unirradiated material. Similarly, one-way ANOVA for the surrogate samples show the quantity of IPDI in the surrogate being an important contributor to Y_{strain} as shown in **Table 4.3**. The significantly lower P value shows that the IPDI added to the surrogate has a notable effect on Y_{strain}.

Table 4.3: One-way ANOVA Results for Surrogate Y_{strain}

Ingredient	F	P value	Significant?
IPDI	19.27	4.2E-05	Yes
HX752	0.53	0.59	No
Aluminum	0.26	0.78	No
Ammonium Sulfate (Coarse)	0.32	0.73	No
Ammonium Sulfate (Fine)	0.13	0.88	No

Combining the one-way ANOVA results show that increasing the quantity of IPDI from low concentration to high concentration affects both Y_{stress} and Y_{strain}. One-way ANOVA also shows that while increasing the quantity of HX-752 is significant for Y_{stress} is not as significant for Y_{strain}. Using the results from the one-way ANOVA to show the importance of IPDI affecting both Y_{stress} and Y_{strain}, two-way ANOVA was then used to further investigate the relationship of the IPDI. Shown in **Table 4.4** are the results using two-way ANOVA for Y_{stress} respective of IPDI. The results show that increasing the quantity of IPDI has effect on Y_{stress} but the interaction of the IPDI with other ingredients is not so significant.

Table 4.4: Two-way ANOVA for Isophorone Diisocyanate on Y_{stress}

Source of Variation	Sum of Squares	Mean of Squares	P-value	Significant?
Quantity	2358.56	1179.28	0.02	Yes
Interaction	12.1	6.05	0.97	No

Similarly, **Table 4.5** shows the two-way ANOVA results for IPDI on Y_{strain}. Increasing IPDI quantity is again a factor affecting Y_{strain}.

Table 4.5: Two-way ANOVA for Isophorone Diisocyanate on Y_{strain}

Source of Variation	Sum of Squares	Mean of Squares	P-value	Significant?
Quantity	61.96	30.95	2.51E-05	Yes
Interaction	1.80	0.90	0.45	No

Results from surrogate sample tests and supporting ANOVA show that increasing the quantities of IPDI by 16% and doubling the quantity of HX-752 will have an effect on Y_{stress}. Similarly, increasing the quantity of IPDI by 16% will also affect Y_{strain}. The combination of the IPDI and HX-752 points to these ingredients as principal contributors in the mechanical performance of the propellant.

4.2 Propellant Phase Results

The propellant phase consisted of evaluating and comparing unirradiated to irradiated specimens of binder, hybrid, and propellant. The binder consists of all the ingredients used in mixing propellant except for aluminum and ammonium perchlorate. The hybrid has the same formulation as propellant with aluminum particles added, but without ammonium perchlorate. The propellant examined is a standard formulation consisting of binder, aluminum particles, and ammonium perchlorate. The MTS computed results for the unirradiated and irradiated baseline binder tensile tests are shown in **Table 4.6**. These results show that at the 6 Mrad reference dose the Y_{stress} value for the baseline case increased considerably, whereas Y_{strain} saw only a marginal gain.

Table 4.6: Comparison of Baseline Unirradiated to Irradiated Binder (6 Mrad)

Parameter	Unirradiated	Irradiated
Y_{stress}	7.4 psi (+/- 0.4 psi)	15.3 psi (+/- 0.4 psi)
Y_{strain}	60% (+/- 2%)	66% (+/- 2%)

The comparison of MTS computed values in **Table 4.6** shows an appreciable increase in Y_{stress} with a marginal increase in Y_{strain} resulting from electron bombardment. The graphical results comparing the baseline case for unirradiated binder to irradiated binder are shown in **Figure 4.2**.

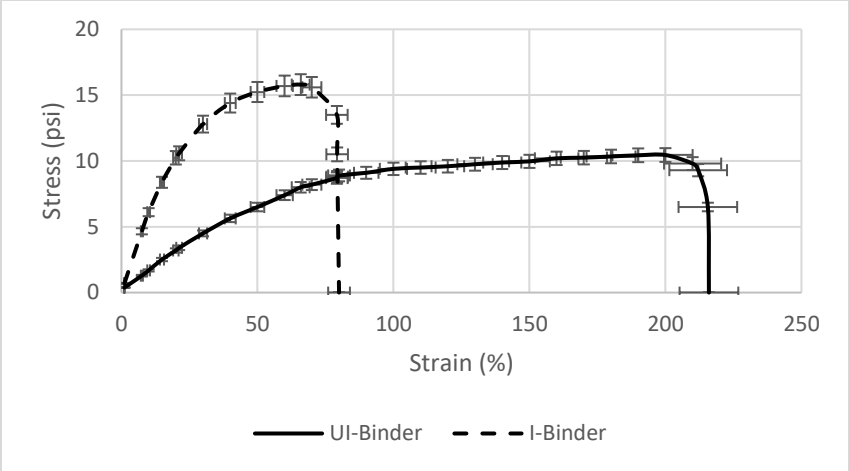

Figure 4.2: Stress – Strain Comparison for Unirradiated & Irradiated Binder (6 Mrad)

A physical effect evident from the radiation exposure was the binder specimens became stiffer and darker in color.

The hybrid specimens were casted and die cut consistent with standard practice and procedure. Hybrid is similar to the propellant with the exception that it has no ammonium perchlorate, only aluminum particles. One of the more visible changes of adding aluminum to the mix is the change in color, from the yellowish color of the cured binder to a grey, metallic looking color. This mix, referred to as hybrid, was mechanically tested before and after irradiation. **Figure 4.3** shows a set of hybrid test specimens after testing with the typical fracture point of the specimens at or near the center of each I-bone.

Figure 4.3: Hybrid Specimens after Testing

This is attributed to the material reaching its maximum tensile strength near the center. Had the samples ruptured at one of the ends or in the grip sections, the failure may have been attributed to improper loading or a pre-existing defect in the material. **Table 4.7** shows the comparison of baseline UI-hybrid to I-hybrid.

Table 4.7: Comparison of Baseline Unirradiated to Irradiated Hybrid (6 Mrad)

Parameter	Unirradiated	Irradiated
Y_{stress}	108 psi (+/- 4 psi)	119 (+/- 4 psi)
Y_{strain}	60% (+/- 2%)	81% (+/- 2%)

The graphical results comparing the baseline case for unirradiated hybrid to irradiated hybrid are shown in **Figure 4.4**.

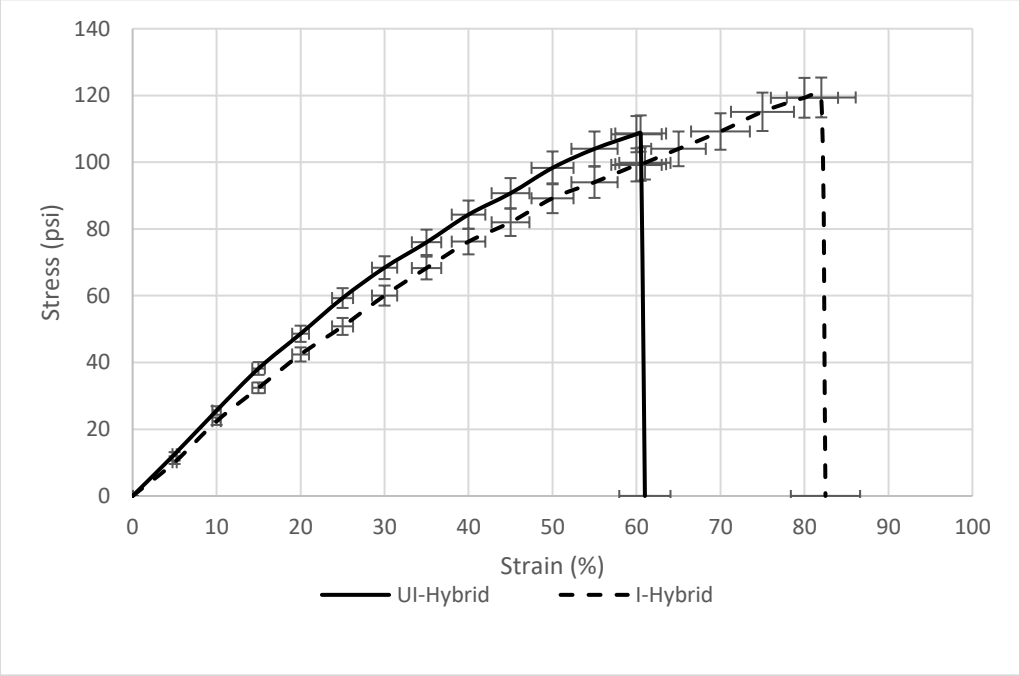

Figure 4.4: Stress – Strain Comparison for Unirradiated & Irradiated Hybrid (6 Mrad)

The comparison of MTS computed values in **Table 4.7** for the hybrid shows a marginal increase in Y_{stress} with a more notable increase in Y_{strain} resulting from electron bombardment. In comparing the results for the irradiated binder and the irradiated hybrid, the effect of the aluminum particles can be seen as minimizing the radiation effects in the material.

Propellant data from a baseline formulation of HTPB propellant was used. **Table 4.8** provides a comparison between the unirradiated and irradiated propellant showing appreciable increases in Y_{stress} and Y_{strain} values.

Table 4.8: Comparison of Baseline Unirradiated to Irradiated Propellant (6 Mrad)

Parameter	Unirradiated	Irradiated
Y_{stress}	115 (+/- 4 psi)	155 (+/- 4 psi)
Y_{strain}	43% (+/- 2%)	62% (+/- 2%)

The graphical results comparing the baseline case for unirradiated propellant to irradiated propellant are shown in **Figure 4.5**.

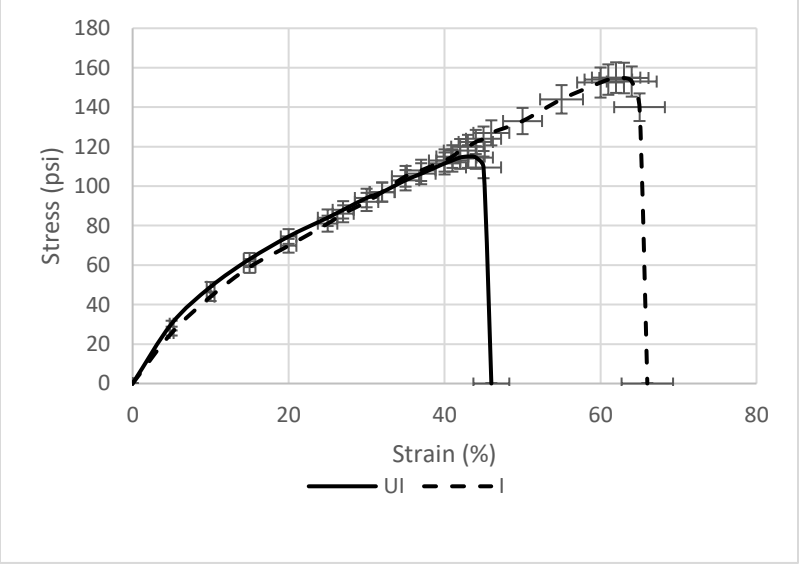

Figure 4.5: Stress – Strain Comparison for Unirradiated & Irradiated Propellant (6 Mrad)

Of interest if the change occurring in the propellant characterized by the transition of the of the Irradiated curve from below the UI to surpassing it at a strain of ~40%. The propellant results point to two important considerations when compared to the hybrid. The first is that of increasing the particulate quantity and the second is that propellant has metallic and non-metallic particle content suggesting different bonding between these and the matrix.

In summary, the results from three types of specimens at a temperature of 77°F consisting of (1) binder; (2) hybrid; and (3) propellant are compared and shown in **Table 4.9**.

Table 4.9: Propellant Phase Baseline Comparison at 77°F (6 Mrad)

Specimen Type	Y_{stress} (psi)	Y_{strain} (%)
UI Binder	7.4 (+/- 0.4)	60 (+/- 2)
I Binder (@6 Mrad)	15.3 (+/- 0.4)	66 (+/- 2)
UI Hybrid	108 (+/- 4)	60 (+/- 2)
I Hybrid (@6 Mrad)	119 (+/- 4)	81 (+/- 2)
UI Propellant	115 (+/- 4)	43 (+/- 2)
I Propellant (@6 Mrad)	155 (+/- 4)	62 (+/- 2)

On the basis of Y_{strain} the unirradiated hybrid samples show reasonable similar values to the actual propellant. However, in the case of the actual propellant Y_{strain} reduces after irradiation, and in the case of the hybrid, Y_{strain} increases. The difference in results between the actual propellant and the hybrid is due to the absence of ammonium perchlorate in the hybrid samples. The reduction in particle content is a significant contributor to the mechanical results.

4.3 Summary of Error

The errors associated with the results can be divided into three parts consisting of errors in preparation, irradiation, and pull testing. Beginning with the preparation of the specimens, errors can enter into the preparation of the specimens due to ingredients, during casting (curing and aging), and during cutting. A summary of potential error during the preparation of specimens is shown in **Table 4.10**. To minimize potential variances during specimen preparation, care was taken to use ingredients that were not past their expiration date and from sealed containers whenever possible. Weights and measures were taken with calibrated instruments as required. Mixing was also conducted with considerable care to avoid the possibility of contaminating mixes with previous loads. Lastly, mitigating variances during cutting was accomplished with the use approved dies and devices specifically dedicated for creating JANNAF specimens.

Table 4.10: Specimen Preparation: Summary of Error

Instrument/Factor	Error	Value Affected
Curing Errors	+/- 0.1% based on HX-752 shelf life & storage temperature	Crosslink Density Chain links
Material Weights & Measures	+/- 0.1% based on product information	Curing process
Mixing Cycle / Process	1% when procedure is followed rigorously	Material properties
Cutting: Dimensional Variation	2% based on cutting accuracy	Dimensions of I-bone flats affecting strain and stress results

With regard to pull testing, the MTS device remains one of the more useful and accurate tools necessary for any type of investigation using I-bone specimens. However, there are a number of errors that can be introduced during its operation that require close attention during the pull testing part of the process. To mitigate potential errors during the pull tested care was taken to ensure specimens were properly placed in the holders. These errors are summarized in **Table 4.11** (also includes error for the scale used for weighing the specimens).

Table 4.11: MTS Model 43 Instrument Error

Instrument/Factor	Error	Value Affected
MTS Model 45 Force Accuracy	+/- 0.5% of applied force	Y_{stress}
MTS Model 45 Speed Accuracy	+/- 0.5% of set speed	Y_{strain}
MTS Model 45 Position Accuracy	Within +/- 0.5%	modulus
MTS Model 45 Strain Accuracy	+/- 0.5% of applied strain	Y_{strain}
Push Action, LLC Digital Scale	+/- 0.1g	Weight, Density

The irradiation process introduced two types of errors, the first is related to having to turn the samples to irradiate them on each side and the second having to do with the

reliance on the Monte Carlo method to determine the dose on the specimens instead of actual radiation measurement.

4.4 SEM Imaging

Scanning Electron Microscope (SEM) images were investigated for the purpose of comparing, to the extent possible, the effects of the ionizing radiation on the materials of interest. Beginning with images of the surrogate, **Figure 4.6** shows the electron microscope scan of a sample of un-pulled and unirradiated material. **Figure 4.6** also shows uniform adhesion between the aluminum particles and the matrix as well as the ammonium sulfate additive.

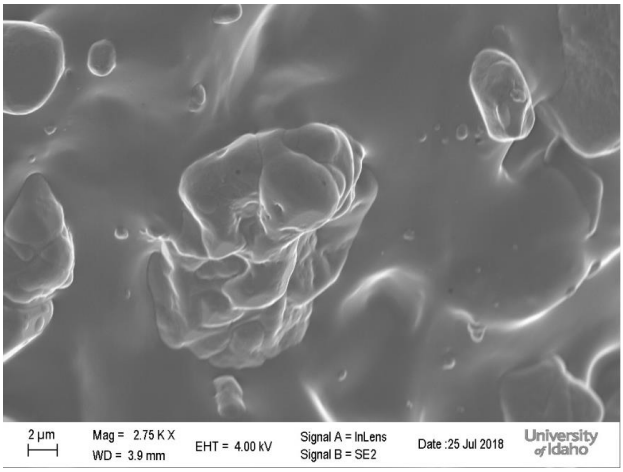

Figure 4.6: SEM Image of Unirradiated Surrogate

Similarly, **Figure 4.7** shows an electron microscope scan of irradiated surrogate.

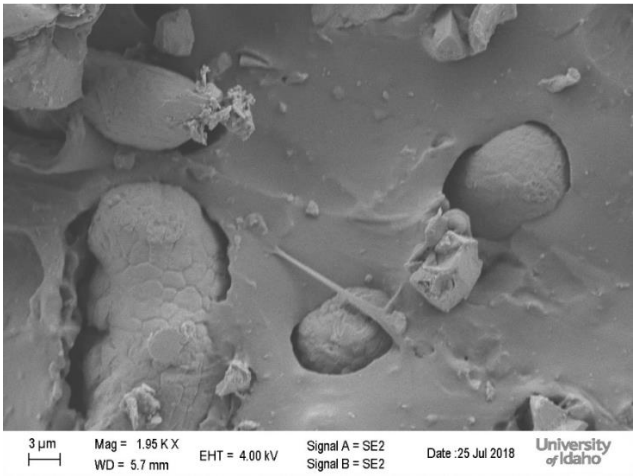

Figure 4.7: SEM Image of Irradiated Surrogate

From **Figure 4.7**, it can be seen that the radiation dose delivered to the specimen caused detachment of the particles from the matrix. This type of relaxation of the structure between the matrix and the particle additives is caused by the dissociation of the hydrogen bonds that form the connections across the network of crosslinks and chains. In **Figure 4.8** below we see yet another type of effect occurring as a result of the radiation dose delivered, which is cleavage of the ammonium sulfate particles.

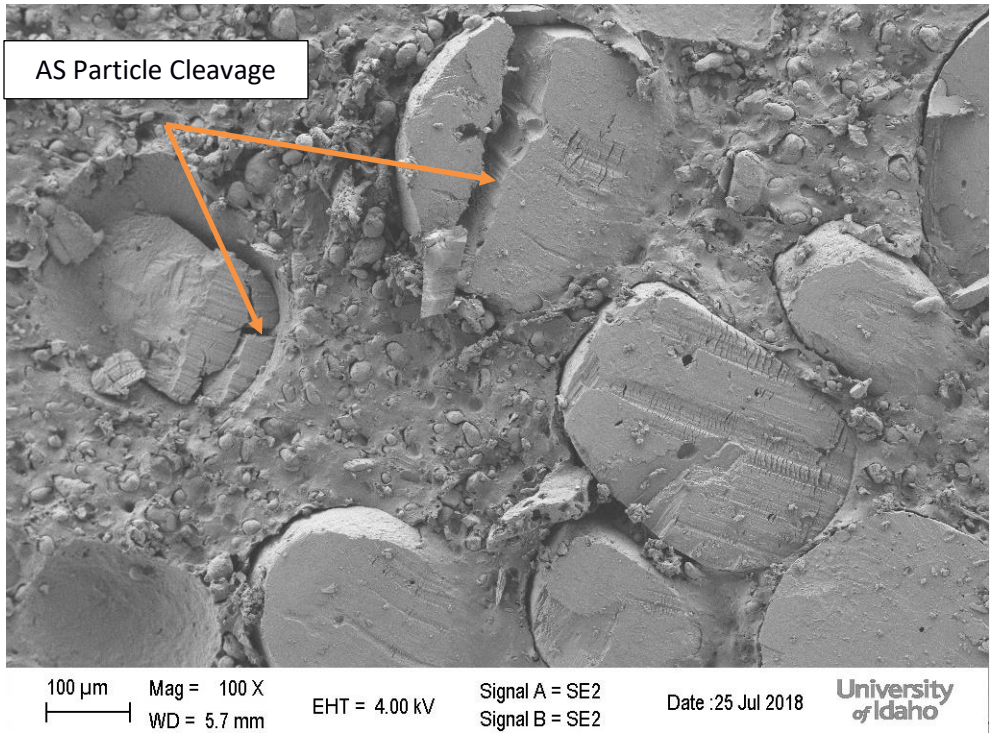

Figure 4.8: SEM Image of Surrogate showing Ammonium Sulfate Particle Cleavage

The effect associated with physical splitting of the AS particles is indicative of a disruption of both types of bonds that exist in the particles considering that there are two types of bonding in ammonium sulfate. Amongst ammonium ions, nitrogen and hydrogen are bonded by covalent bonds, which are essentially intermolecular-van der Waals forces, as both nitrogen and hydrogen are non-metals. However, ammonium and sulphate ions are joined together by ionic bonds.

Crosslinking is the formation of chemical side bonds between the network of chains in a polymer. **Figure 4.9** is an electron microscope scan of crosslinks in a region of pure unirradiated and un-pulled HTPB binder showing the network of crosslinks connecting chains in the binder in the absence of particle additives.

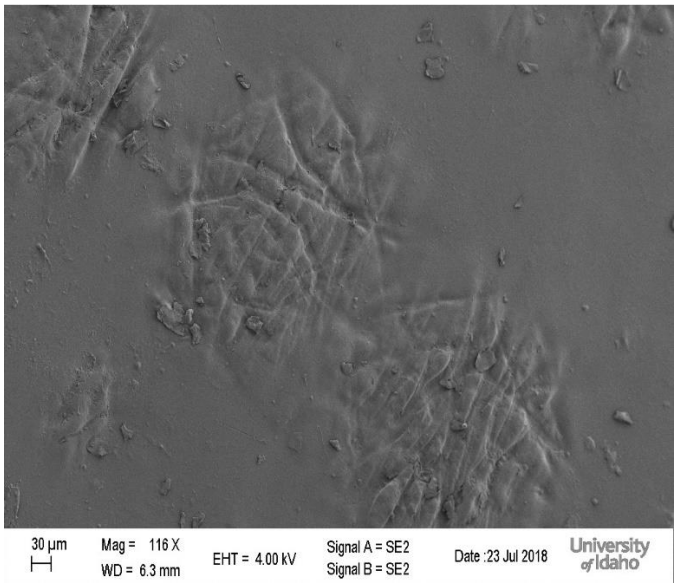

Figure 4.9: SEM Image of Unirradiated HTPB Binder

In contrast, **Figure 4.10** shows an electron microscope scan of the same region in the binder after being irradiated in the Pelletron with 2 MeV electrons delivering a dose of 6 Mrad. This image shows how electron bombardment rearranged the crosslinks in the binder.

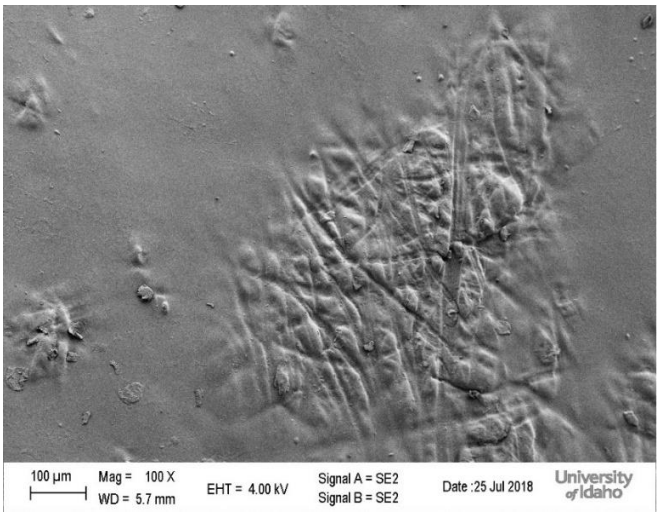

Figure 4.10: SEM Image of Irradiated HTPB Binder

The connection of chains through crosslinking serves to increase the rigidity of polymer while maintaining some elastomeric properties. Understanding cross-link density is essential to understanding the effects that radiation has on polymer structure because the path that electrons travel in the matrix disrupt the connections of the polymer chains and the forces that enable crosslinks to enhance the strength and elastic properties of the propellant.

An SEM image taken at the University of Idaho of the unirradiated hybrid sample is shown in **Figure 4.11**, where the unirradiated material can be seen uniformly bonding to the particles.

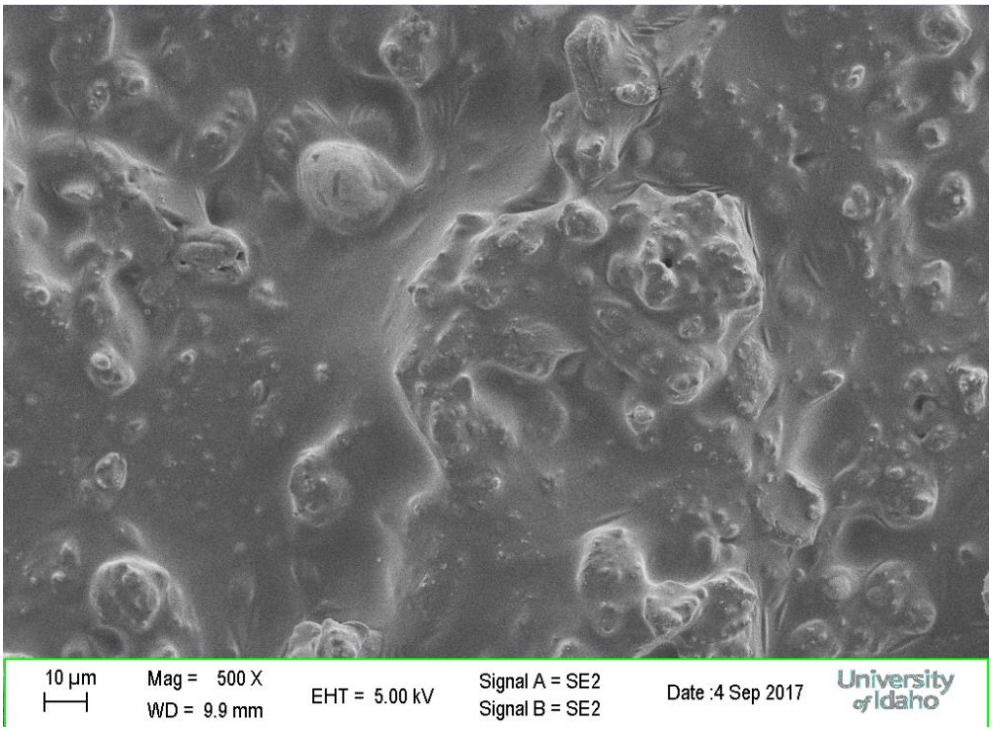

Figure 4.11: SEM Image of Unirradiated Hybrid

However, in **Figure 4.12**, an electron microscope scan image shows the changes to the material after exposure to electron radiation. **Figures 4.11** and **Figure 4.12** were taken from two different specimens of the same composition respective of similar locations on the specimens in an effort to achieve a uniform visual comparison between irradiated and unirradiated samples.

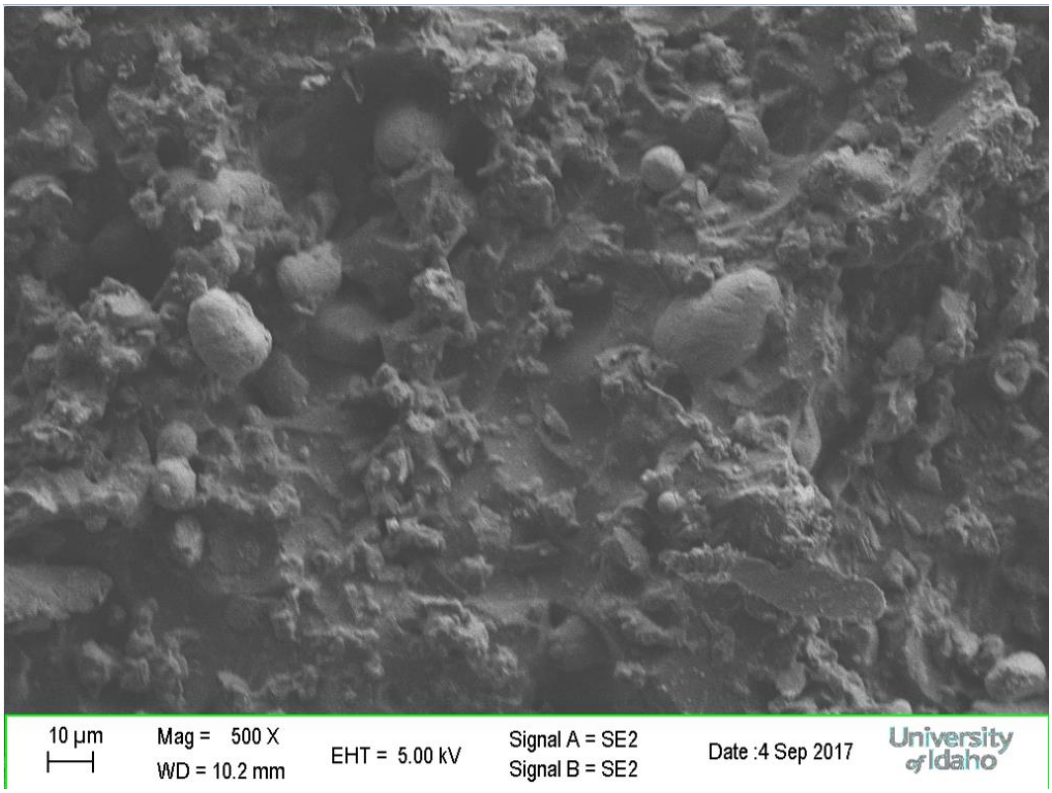

Figure 4.12: SEM Image of Irradiated Hybrid

The effects of radiation on the matrix can be considered as a disruption of the curing process of the propellant in that the original network of polymer links achieved during curing is effectively disrupted and rearranged.

Ionizing radiation also affects the mechanical properties of a propellant by weakening the ionic bonds between the aluminum particles and the matrix. When electrons interact in the region where the particle is in contact with the matrix, the bonds weaken causing a detachment of the aluminum particles. SEM scans show aluminum particles loosening and dislodging from their locations. This is significant because the matrix' mechanical properties rely on its ability to transfer load to the aluminum particles, which are capable of bearing greater tensile forces. Once weakened or dislodged, the effective contribution of the particles to the load bearing properties of the propellant are reduced. Another important observation from **Figure 4.12** is the occurrence of off-gassing where hydrogen is released during interactions with the electrons. The work by Singh elucidates the effect of ion beam irradiation on

metal particle doped polymer composites (Singh, et al., 2011) providing further evidence of the off-gassing that results from polymer exposure to ionizing radiation. Singh reports that for polymethyl methacrylate (PMMA) with Ni powder additive, ion bombardment led to converting the polymer structure into a hydrogen depleted carbon network. Singh attributes this to the rupture of polymeric bonds resulting in the emission of hydrogen. **Figure 4.13** below shows SEM images (magnification = 1.00K x) of hydrogen off-gassing resulting from ion bombardment of a non-particle composite PMMA polymer with 10% Ni.

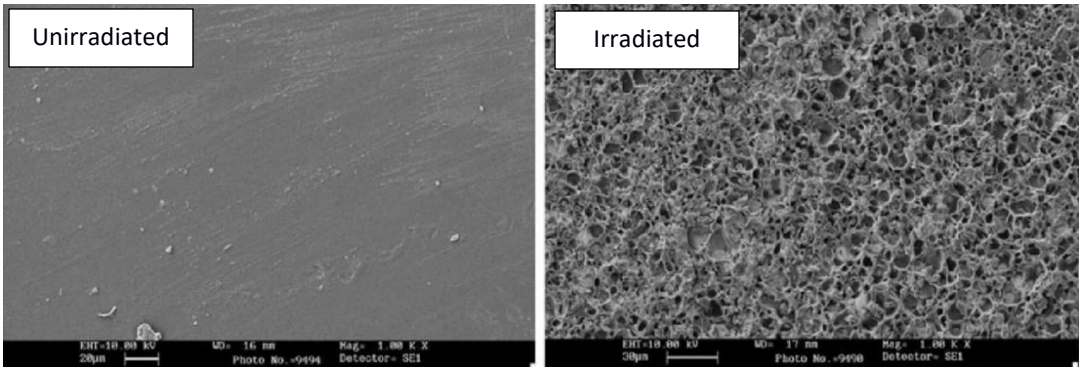

Figure 4.13: Off-gassing from Irradiation of Polymethyl Methacrylate w/10%Ni (Singh, 2011)

Similarly, **Figure 4.14** shows SEM images (magnification = 1.00K x) of hydrogen off-gassing resulting from ion bombardment of PMMA polymer with 40w% Ni. A comparison of these images shows considerable change in morphology as a result of irradiation in both the 10w% and 40w% Ni additive.

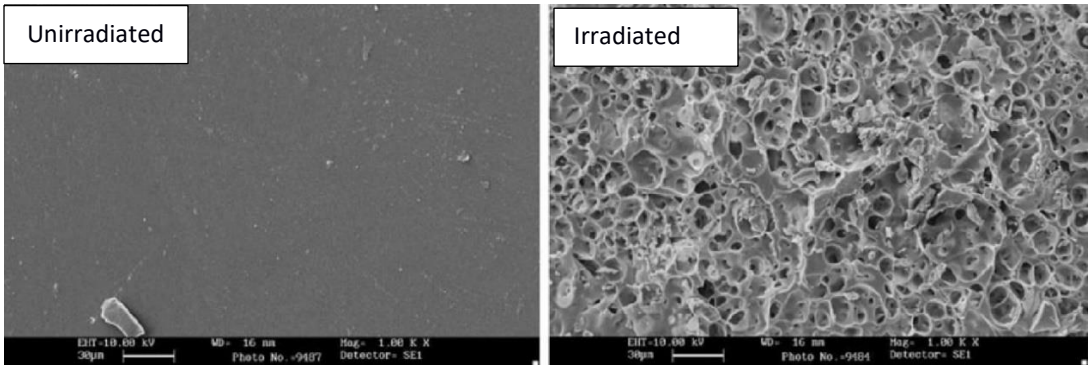

Figure 4.14: Off-gassing from Irradiation of Polymethyl Methacrylate w/40%Ni (Singh, 2011)

While the work by Singh is not of HTPB or its radiation effects, it provides a comparison of a key reaction that is associated with off-gassing due to the release of hydrogen during interactions with electrons.

Chapter 5. Analysis

The transfer of energy from electrons to the propellant occurs over a wide range of energy as they pass through and interact within the propellant. Electrons change the material's molecular structure through each interaction that occurs, where energy is transferred to the struck molecule, resulting in broken or altered bonds. Ionizing radiation causes chemical degradation in polymers and consists mainly of crosslinking, chain scissoring, changes in the number and type of double bonds and the emission of low molecular weight gaseous products. Polymers whose primary reaction to ionizing radiation is crosslinking typically see some improvement in mechanical properties (Kornacka, 2017). For polymers whose principal reaction is chain scission, the principal results are low molecular weight fragments, gas evolution and unsaturated bonds. In these processes free radicals determine the initiating centers for scissioning and crosslinking. Chemical bonds exist as a result of the attraction created by the transferring or sharing of valence electrons. Molecular effects resulting from exposure to ionizing radiation necessitates understanding both ionic and covalent bonds in the study of HTPB bond structure. Ionic bonds are significant as these are typically characterized by metal to non-metal bonding, as is the case between the aluminum particles and the matrix. Being covalent bonds typically exist between a non-metal and a non-metal, covalent bonding is important respective of the bonds that constitute the matrix.

There are three primary nuclear mechanisms that play a role in how the chemical properties of the propellant are changed. These are (1) ionization; (2) Bremsstrahlung; and (3) elastic scattering. There are two principal radiation effects are of particular interest in relation to how the grain is expected to behave during its travel to Europa. First, exposure to ionizing radiation is expected to cause a combination of molecular changes that depending on the energy of the incident particles and the dose deposited, will lead to changes in surface topography and the creation of voids around the fuel and oxidizer particles. This weakening of the matrix in the zone surrounding the particles will lead to debonding. Second, exposure to radiation causes a rearrangement of the

connections between polymer chains effectively altering the molecular weight of the propellant. **Table 5.1** provides a summary of effects from charged particle radiation.

Table 5.1: Effects from Charged Particle Radiation

Level	Primary Effect	Consequence	Significance
Atomic Level	Electrons gradually lose energy passing through the grain. As electrons pass through the grain the energy from them is dissipated by excitation or ionization of the atoms or molecules they come in contact with.	These interactions lead to changes in physical and chemical properties	In the case of polymers, excitation and ionization leads to gas evolution, polymerization, crosslinking, degradation and double bond formation, where these have a direct effect on physical properties
Molecular Level	Chain scission	Molecules in the grain being broken into smaller fragments	Scission takes place in polymers having a carbon tetra
	Crosslinking (both crosslinking and degradation occur simultaneously	Formation of larger molecules and in a different network arrangement than originally cured	Polymers preferentially crosslink or degrade depending on their chemical structure. In polymers with carbon chains crosslinking occurs when a carbon molecule carries at least one hydrogen atom
Material Level	Certain additives have a protective action and can reduce the effects of radiation on polymers	These additives may be energy absorbers or chemical reactants that combine with radiation produced free radicals.	When combined with mechanical forces exposure to ionizing radiation induces cleavage of oxidizer particles at lower radiation doses. Surface morphology also raises propensity for cracking leading to potential instability of the propellant resulting from changes in burn area inside the combustion chamber.

Changes to the uniformity of the propellant and its density are important considerations because they can affect the stability of the propellant during ignition and burning. The observed changes in topography from the SEM scans of the hybrid point to changes in uniformity, which are important respective of propellant burn area (A_b). The change in material density may make the propellant more susceptible to cracks, which will in turn also affect the burn area in the combustion chamber of the rocket motor. Changes in molecular weight bear consideration in relation to propellant

density, where the chain scission contributes to a reduction in molecular weight due to what is effectively a damage mechanism that becomes more dominant at higher doses. A typical motor chamber pressure curve is shown in **Figure 5.1** consisting of transient and steady state stages. The transient stages consist of the startup, where the propellant ignites and causes chamber pressure to rise very quickly, and the tail-off, where the chamber pressure decreases to ambient level.

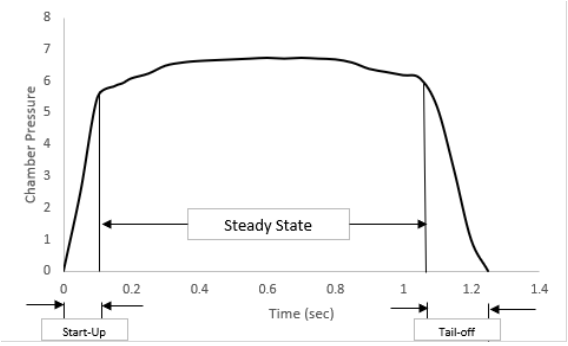

Figure 5.1: Typical Motor Chamber Pressure

The area in between the two transient stages is the steady state stage where variations in chamber pressure are due primarily to variation in grain geometry, which corresponds to burning surface area with a corresponding variation in burn rate. In understanding the start-up pressure rise and the steady state pressure stage, the rate of combustion product generation is proportional to the rate of consumption of the propellant grain as given by,

$$\left(\frac{dm}{dt}\right)_g = A_b\, \rho_p\, r \qquad 5.1$$

Where ρ_p is the propellant density, A_b is the grain burning area, and r is the propellant burn rate. In addition to the changes in propellant density caused by radiation exposure, changes to the propellant burning area are of more significant concern, as these changes could lead to instability due to cracks. The presence of cracks in the grain during and after ignition may lead to changes in burning rate that could in turn diminish the performance of a deceleration motor. An additional consideration that may affect

burn rate is particle debonding. Once the particles are no longer suspended in the matrix, when ignited the fuel may burn too fast or simply not burn with the same efficiency as when initially casted. The resulting changes in burn rate can affect the performance of the deceleration motor potentially rendering it unable to slow the spacecraft down sufficiently to deploy a lander.

The evaluation of crosslink density is necessary in the understanding of the radiation effects from electron bombardment and is normally associated as an important mechanism at multiple radiation doses. At a macroscopic level, a cross-link connects one polymer chain to another and as such, cross-linking refers to the connection of polymer chains. When a cross-linking agent is added to a solid propellant to form a rubber-like solid, cross-linking normally results in a decrease in flexibility (decrease in strain), an increase in hardness and strength and an increase in the melting point of the propellant. When propellant chains are crosslinked, they are not able to shift as easily under mechanical loads. The resulting mechanical properties of the propellant become highly dependent on the number of active cross-links.

In this dissertation two of the more common models for predicting crosslink density are used to derive a relationship between crosslink density and radiation dose on the basis of Y_{stress} and Y_{strain} measurements. The first of these methods is the Flory – Rehner method and it is based on a Gaussian distribution of crosslinks as defined by,

$$\sigma = v_e \, RT \, (\tilde{\lambda} - \tilde{\lambda}^{-2}) \qquad 5.2$$

In the Flory – Rehner relationship, σ is the stress, R is the universal gas constant, T is the reference temperature, and $\tilde{\lambda}$ is the extension ratio. The results of the Flory – Rehner relationship on the basis of radiation dose for the propellant are shown in graphical form in **Figure 5.2**, noting that the crosslink density values corresponding to

the dose increments between 0 and 6 Mrad were obtained using the Monte Carlo method described in Appendix B.

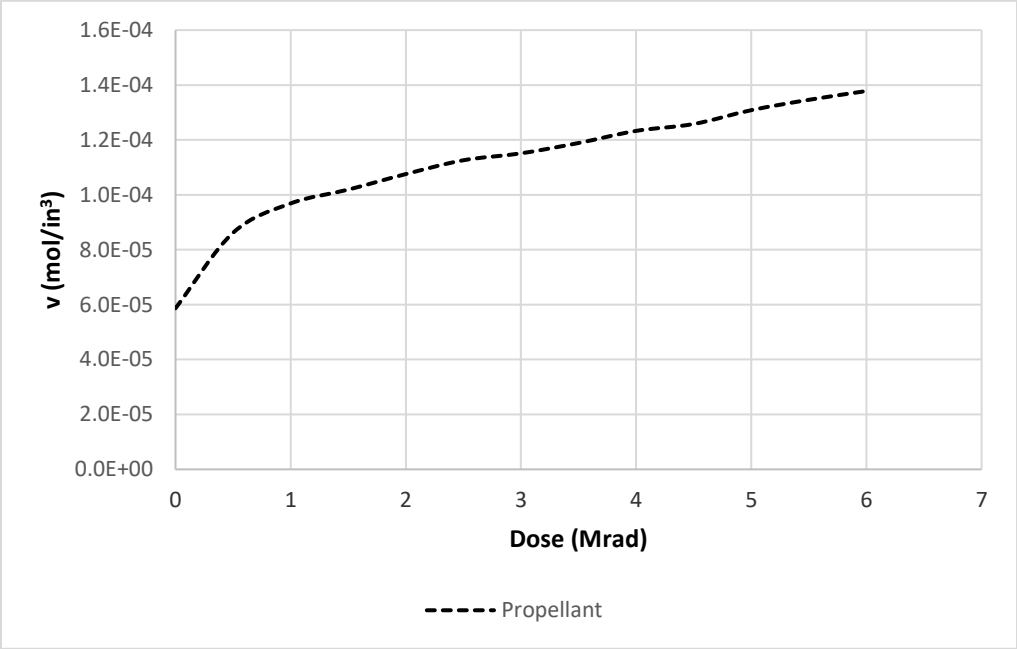

Figure 5.2: Propellant Crosslink Density vs Dose (Flory – Rehner model)

While the Flory – Rehner model can over predict the value of crosslink density, it serves to show the relationship for how the number of crosslinks increases as a result of electron bombardment. During mixing, the crosslink density is controlled by the amount of prepolymer 'diol' present in the hydroxyl terminated polybutadiene binder, and the addition of aziridine (HX-752) and isophorone diisocyanate (IPDI). The combination of these ingredients working together provide the network of bonds that culminate in the curing process. Therefore, an evaluation of crosslink density is important because it serves to develop an understanding of radiation effects at the molecular level from mechanical data resulting from I-bone pull tests. Crosslink density corresponds to the number of crosslinks per unit volume of propellant and affects the propellant's material properties after cure. Crosslink density depends on four factors that include (1) number of functional sites in the propellant; (2) the molecular distance between these functional sites; (3) the chain mobility between

functional sites; and (4) the percentage of these sites that react as part of the curing process.

The second method used in this dissertation to predict crosslink density is the Mooney – Rivlin model. The Mooney – Rivlin model uses non-Gaussian statistical theory and is expressed in the following form,

$$2C_1 + \frac{2C_2}{\lambda} = \frac{\sigma}{(\lambda - \lambda^{-2})} \quad 5.3$$

In Equation 5.3, C_1 and C_2 are independent parameters, where the term C_1 is defined as a Gaussian term by,

$$C_1 = \frac{1}{2} v_e RT \quad 5.4$$

The term C_2 in Equation 5.3 represents those factors causing a material to differ from Gaussian statistical predictions corresponding to worm-like networks as discussed in the early work by Kratky & Porod in 1943. The computed value for C_2 for propellant is shown graphically as a function of radiation dose in **Figure 5.3**.

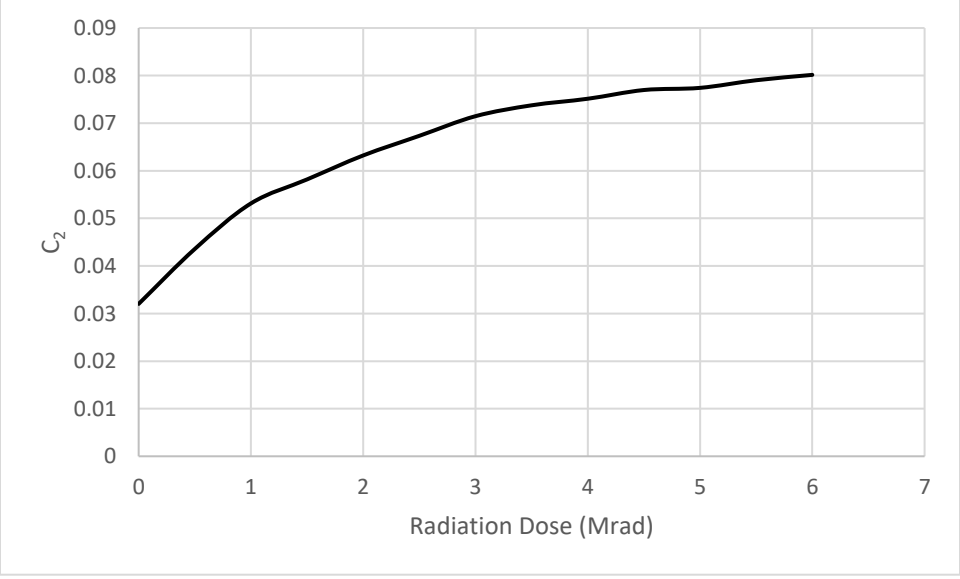

Figure 5.3: C_2 Value for Propellant vs Dose (Mooney – Rivlin model)

The results of the Mooney – Rivlin model for the crosslink density are shown in **Figure 5.4.** The results show the crosslink density increasing as a function of radiation dose. While the predicted values for crosslink density are approximately an order of magnitude lower in comparison to the Mooney – Rivlin model, **Figure 5.4** shows a significant increase in crosslink density as a result of the 6 Mrad reference dose.

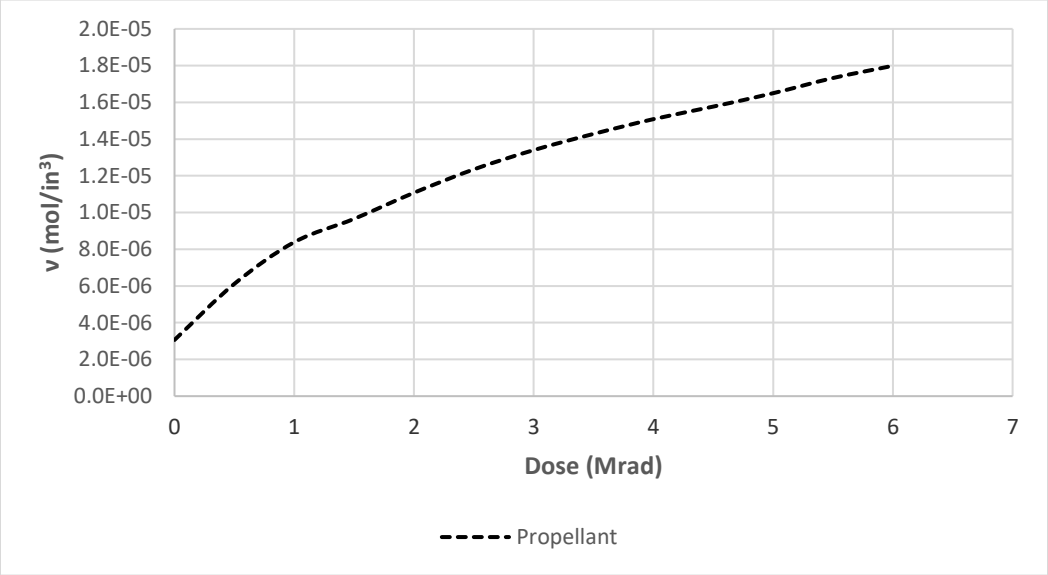

Figure 5.4: Propellant Crosslink Density vs Dose (Mooney – Rivlin model)

The Goodier model (Goodier, 1933) provides a method to determine tensile stresses in unfilled and filled polymers with particles. This method assumes that the polymer yield point is the point of maximum plastic deformation. The work by Goodier also asserts that the load carried by the matrix and the filler corresponds to their cross sections. In the Goodier method, the cross section in a tensile specimen for the matrix is given by,

$$C_m = 1 - [1.21\left(Vp^{\frac{2}{3}}\right)] \quad 5.5$$

Conversely, the cross section for the particles in the specimen is given by,

$$C_p = 1.21(Vp^{\frac{2}{3}}) \quad 5.6$$

When combined with a fundamental assumption by Goodier that the average stress acting across the surface of the fillers is given by σ_p, the relationships in Equation 5.5 and Equation 5.6 form the basis for the following relationship for the composite stress σ_c,

$$\sigma_c = \sigma_m \left[1 - 1.21\left(Vp^{\frac{2}{3}}\right)\right] + \sigma_p[1.21\left(Vp^{\frac{2}{3}}\right)] \quad 5.7$$

Where σ_c is the tensile stress of the composite and σ_m is the tensile stress of the matrix. The load carried by the filler σ_p was found by Goodier to be smaller than σ_m when large particles are used in the mix and debonding increases as a result. The work by Goodier provides insight into understanding how the surface area of the filler is larger when smaller particles are present and the resulting value for σ_p can exceed the value for σ_m.

For composites with a high concentration of small particles the computed values for σ_p using the Goodier model produces values well above the Y_{stress} of the composite. This is because for very high concentrations of small particles, where small particles make up a considerable quantity of the composite, the value for σ_p resembles that of a solid. So, in the case of high particle content, with a high concentration of small particles, it is necessary to introduce a correction to Equation 5.7 to normalize the value for σ_p to be representative of the recorded values for σ_c and σ_m. This correction yields a value for the load on the particle in the form of σ'_p given by,

$$\frac{\sigma_p}{(\sigma_c/\sigma_m)} = \sigma'_p \quad 5.8$$

This correction introduces an approximation that falls well within the measured values for the propellant (σ_c) and for the binder (σ_m). The results for Y_{stress} of the binder

presented in this investigation provide the needed values for σ_m to enable the aforementioned approximation to be performed. The results of Equation 5.8 are plotted and shown in **Figure 5.5** on the basis of radiation dose.

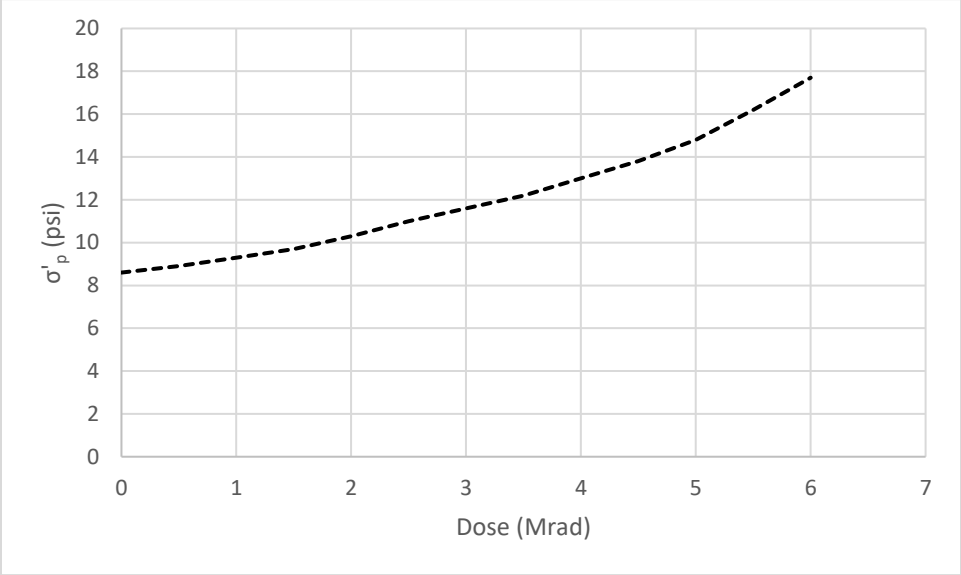

Figure 5.5: Load Carried by Particles (Goodier model)

The work by Goodier led Pukansky and his team to expand the relationship to investigate the degree of particle to matrix reinforcement. The Pukansky relationship (Pukansky, 1993) is given by,

$$\sigma_c = \sigma_m\left[\frac{1-Vp}{1+2.5Vp}e^{BVp}\right] \qquad 5.9$$

In this equation, *B* is an experimental parameter representing the particle / matrix reinforcement for the propellant in this investigation. The value of *B* increases with the surface area and the adhesive strength of the filler polymer interface. The results for the propellant using the Pukansky model suggest that small particles improve interfacial stress transfer in the propellant. The results for bonding factor (*B*) using the Pukansky model as a function of radiation dose are shown graphically in **Figure 5.6**.

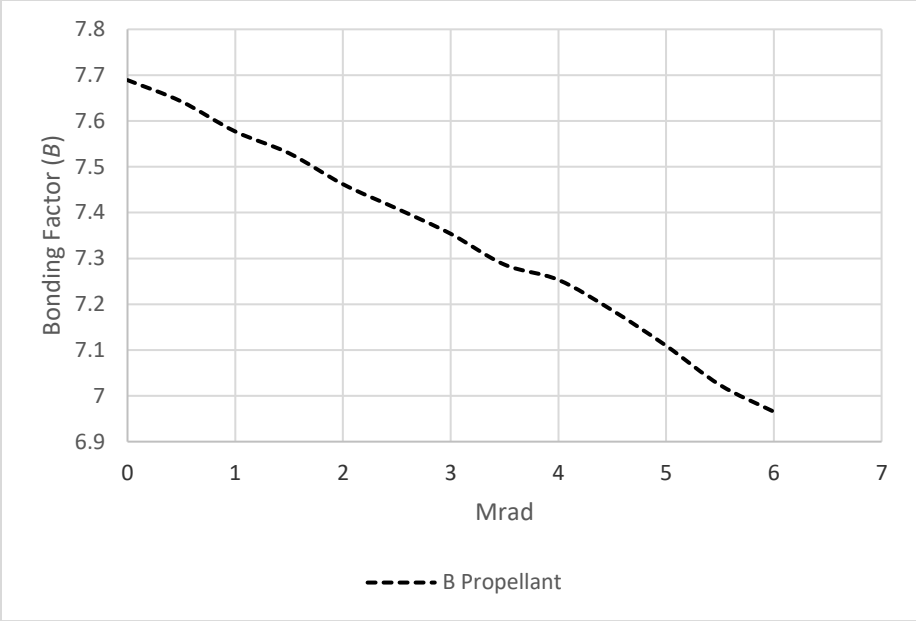

Figure 5.6: Particle Bonding (*B*) as a Function of Radiation Dose (Pukansky model)

The results from Pukansky paved the way for Nicolasis and Narkis to propose a new theory that relates composite Y_{stress} with the Y_{stress} of the matrix and the volume fraction of the filler (Nicolasis & Narkis, 1971). Therefore, the Nicolasis and Narkis equation takes the following form,

$$\sigma_c = \sigma_m \left(1 - K\left(Vp^{\frac{2}{3}}\right)\right) \qquad 5.10$$

Where once again, σ_c represents Y_{stress} of the composite and σ_m represents the Y_{stress} of the matrix and V_p is the volume fraction of the filler. The parameter *K* in the Nicolasis & Narkis equation accounts for the adhesion between filler particles and the matrix. The lower the value of *K* the better the adhesion. The work by Nicolasis and Narkis shows that the value of *K* for poor adhesion is ~1.21. However, the values of *K* reported by Nicolasis & Narkis in their work typically range between 0.2 and 1.0. The results of the Nicolasis and Narkis model are shown graphically in **Figure 5.7** where it is demonstrated that as radiation dose increases the adhesion parameter *K* increases indicating a reduction in the adhesion of the particles with increasing radiation dose.

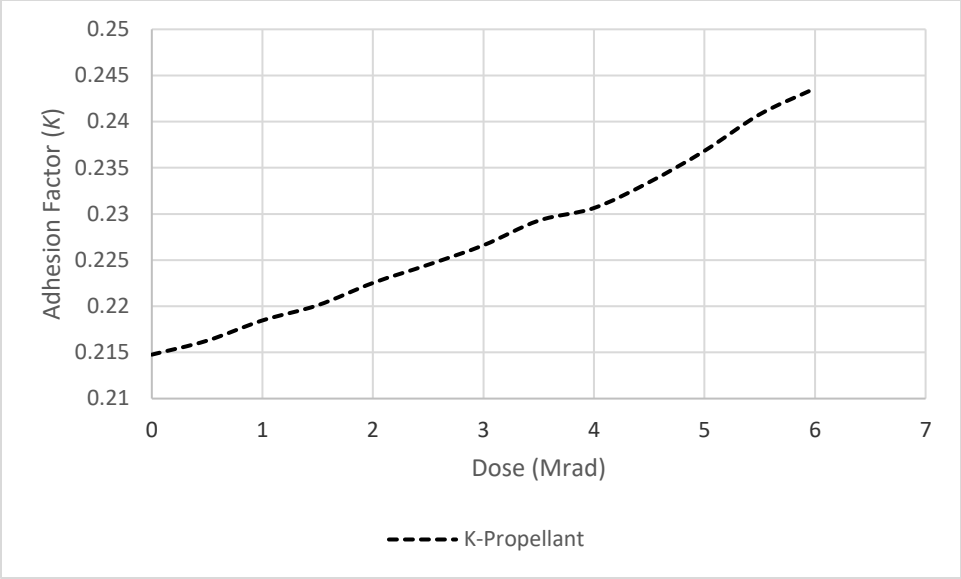

Figure 5.7: Adhesion Factor (*K*) as a Function of Dose (Nicolasis – Narkis model)

The Pukansky and Nicolasis – Narkis models assume three basic conditions consisting of (1) the matrix and filler having no appreciable amount of chemical interaction only physical; (2) that the matrix is stiffened with the addition of particle filler; and (3) that the change in modulus is primarily due to the size of the particles added to the matrix.

A study by Matonis & Small (1969) revealed that filler particles can act as initiation sites during the solidification process where these initiation sites are surrounded by a higher concentration of polymer bonds leading to an increased modulus. However, the zone immediately adjacent to this higher modulus layer is expected to have a zone of material with a lower modulus. This suggests that large particles have a decreasing effect on the Young's modulus of the matrix. Investigations by Valavala & Odegard (2005) suggest that (1) particles restrict the mobility and deformability of the matrix by introducing a mechanical restraint, the degree of which depends on the spacing between particles and the bonding between the particle and the matrix; (2) restriction in polymer molecular diffusion is seen in the presence of solid particles; and (3) particulate filled composites have poor stress transfer at the filler-polymer interface because of the non-adherence of the filler to the polymer. Combined, these

mechanisms affect propellant stability, which pose significant challenges to the deceleration motor.

The tensile test results from both the surrogate phase and propellant phase were used develop several relationships to determine radiation sensitivity for propellant crosslink density, particle loading and particle adhesion – debonding as shown in **Figure 5.8**. The models employed relied on three relationships. The first was between mechanical performance and crosslink density, particle loading and adhesion – debonding. The second was between radiation dose and mechanical performance. The third was between radiation dose and crosslink density, particle loading and adhesion – debonding.

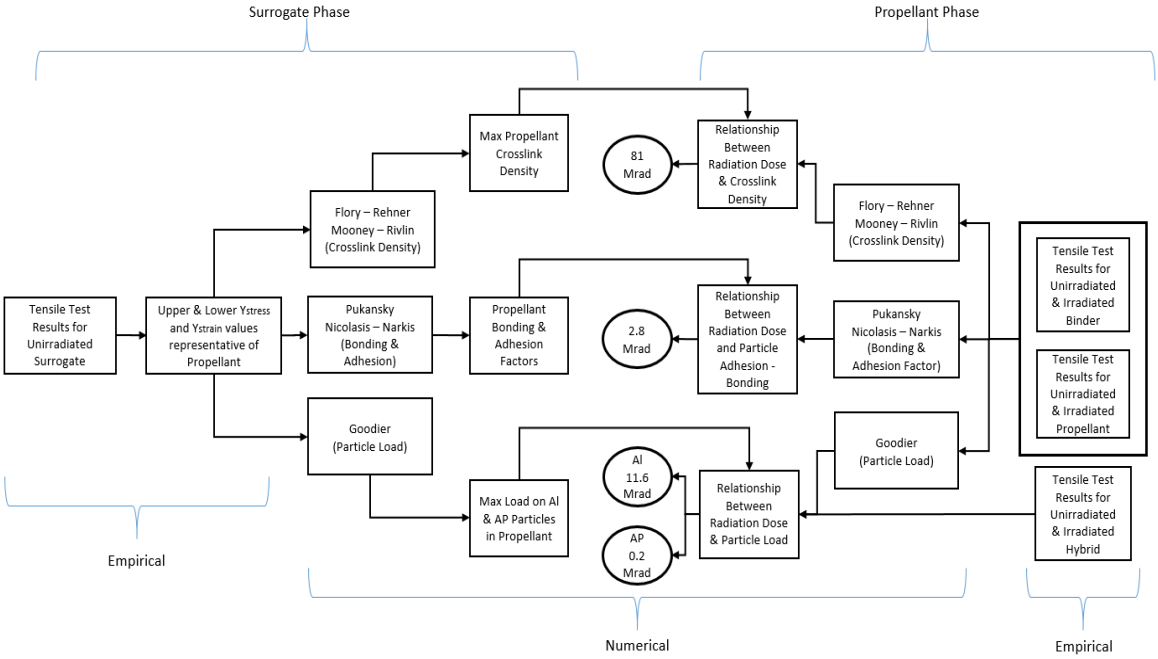

Figure 5.8: Relationship between Numerical & Empirical Methods

The surrogate phase provided a range of representative values for propellant upper Y_{stress} (173 psi) and Y_{strain} (65%) and lower Y_{stress} (115 psi) and Y_{strain} (20%). These upper and lower values were used with the methods shown in **Figure 5.8** and **Table 5.2** to obtain limiting values for propellant crosslink density, particle loading and adhesion – bonding.

Table 5.2: Summary of Results

Component	Propellant Limiting Value	Corresponding Dose (Mrad)	Method
Crosslink Density	1.7E-04 mol/in^3	81	Mooney-Rivlin
Load on the Aluminum	37 psi	11.6	Goodier
Debonding & Adhesion	7.5 (*B*) 0.23 (*K*)	2.8	Pukansky (*B*) Nicolasis/Narkis (*K*)
Load on the ammonium perchlorate	9.3 psi	0.2	Goodier

As shown in **Figure 5.8**, the limiting values for the propellant were used with the relationships derived from the propellant phase for unirradiated and irradiated specimens to obtain values for radiation dose. It is seen from the results obtained and shown in **Figure 5.8** and **Table 5.2** that while bonding and adhesion are close to the required 2.4 Mrad value, it is the Ammonium Perchlorate that has the higher radiation sensitivity of the propellant characteristics studied (0.2 Mrad). These results indicate that the Ammonium Perchlorate is below the required radiation tolerance of 2.4 Mrad for the mission.

Chapter 6. Conclusions

Significant progress was made toward investigating the radiation sensitivity of HTPB propellant with regards to radiation effects on propellant binder, the aluminum and ammonium perchlorate using models for crosslink density determination, bonding and adhesion and values for mechanical load on the aluminum and the ammonium perchlorate. The results of this investigation show that a future mission to Europa could exceed the radiation dose permissible by the current design of the Europa Braking Motor. Based on Y_{stress} and Y_{strain} values of typical HTPB propellant formulations a series of models were employed to derive the corresponding dose to the propellant on the basis of crosslink density, particle bonding and adhesion, and load capacity of the particles. The assessment of these aspects of the propellant show that based on the load characteristics of the ammonium perchlorate, it will have the highest radiation sensitivity under the parameters investigated in this dissertation. While previous investigations by others to assess radiation damage of ammonium perchlorate show corresponding dose values higher than the values reported in this effort, those efforts omitted consideration to mechanical forces.

The current concept for the EBM design calls for a higher anticipated radiation dose to the systems onboard than what is determined in this dissertation for the ammonium perchlorate in the propellant, and as a result warrants further investigation to determine how the propellant can be shielded. The values reported in this investigation reflect radiation effects on the propellant, combined with mechanical forces representative of foreseeable conditions during space travel. The findings of previous investigations into radiation effects on ammonium perchlorate, when combined with the findings reported and elucidated in this dissertation for the propellant as a whole, provide the foundation for continued efforts leading to greater confidence in the performance of the propellant and of a future Europa Breaking Motor design. The ability of the propellant to meet mission requirements could depend on incorporating shielding in the casing of the EBM.

References

Abadchi, M. R., Jalali-Arani, A., The Use of Gamma Irradiation in Preparation of Polybutadiene Rubber Nanopower; Its Effect on Particle Size, Morphology and Crosslink Structure of the Powder, November 11. 2013

Aerojet General Co., Study of Mechanical Properties of Solid Rocket Propellant, Report Number 0411-10Q-1, Sacramento, CA May 30, 1961

Ahmed, S., Jones, F. R., A Review of Particle Reinforcement Theories for Polymer Composites, Journal of Materials Science, Volume 25, 1990

Al-Haik, M. S., et al., Nano-characterization of Proton Radiation Damage on Magnetically Oriented Epoxy, International Journal of polymer Analytical Characteristics, Volume 12, Pg. 413-430, Taylor & Francis Group, LLC, 2007

Allan, W. D., et al., HTPB Polymer Improvement, Report AD-750 551, Lockheed Propulsion Co., Air Force Rocket Propulsion Lab, September 1972

Anglin, J. D., et al., Trapped Energetic Ions in Jupiter's Inner Magnetosphere, Journal of Geophysical Research, 1997

Anuar, H., et al., Effects of Electron Beam Irradiation on Mechanical Properties of PP/EPDM Nanocomposites, Journal of Rubber Research, Volume 14(3), 2011

Assink, R. A., et al., Thermal Degradation Studies of Polyurethane Propellant Binder, Sandia National Labs, Albuquerque, NM June 12, 1999

Azoug, A., et al., Microstructure and Deformation Mechanisms of a Solid Propellant Using 1H NMR Spectroscopy, Fuel Journal, Volume 148, Pg. 39-47, May 15, 2015

Bencher, C. D., et al., Microstructural Damage and Fracture Processes in a Composite Solid Rocket Propellant, Journal of Spacecraft and Rockets, Volume 32, Number 2, March – April 1995

Bethe, H. A., Zur Theorie des Durchgangs schneller Korpuskularstrahlen durch Materie, Ann. d. Physik volume 5, Pg. 325, 1930

Bethe, H. A., Bremsformel für Elektronen relativistischer Geschwindigkeit, Z. Phys. Volume 76, Pg. 293, 1932

Beyer, R., Graham, P., Hyperplastic Behavior of Solid Rocket Propellants, NASA Technical Brief MFS-28880, NASA Marshall Space Flight Center, June 01, 1995

Bhowmick, A. K., Vijayabaskar, J., Electron Beam Curing of Elastomers, Rubber Chemistry and Technology, Volume 79, Number 3, Pg. 402-428, July 2006

Bourdarie, S., Sicard, A., Physical Electron Belt Model from Jupiter's Surface to the Orbit of Europa, Journal of Geophysical Research Atmosphere, Vol. 109, February 2004

Brodnyan, J., Particle Reinforcement for Polymer Composites, Transactions of the Society of Rheology, American Institute of Physics, Volume 6, 1959

Bustamante, C., et al., Entropic Elasticity of Lambda Phase DNA, Science, 265, Pg. 1599, 1994

Calhoun, A., Peacock, A., Polymer Chemistry – Properties & Applications, Hanser Publishers, Munich, 2006

Chang, K. C., Kamaratos, E., Theoretical Studies of Radiation Effects in Composite Materials for Space Use, NASA Contractor Report 3618, Langley Research Center, 1982

Chapiro, A., Radiation Chemistry of Polymeric Systems, Wiley Interscience, New York, 1962

Chemical Propulsion Information Agency (CPIA), Solid Propellant Mechanical Behavior Manual, CPIA Publication 21, JANNAF Interagency Propulsion Committee, Interagency Chemical Rocket Propulsion Group, Johns Hopkins University, APL, Laurel, MD, 1988

Cheng, S., et al., Improving Processability of Polyethylene by Radiation Induced Long Chain Branching, Radiation Physics and Chemistry, Volume 78, Issues 7-8, Pg. 563-566, August 2009

Cherng, M., et al., Optimum Shielding in Jovian Radiation Environment, Nuclear Instruments and Methods in Physics Research, Section A: Accelerators, Spectrometers, Detectors and Associated Equipment, Volume 580, Issue 1, Pg. 633-636, September 21, 2007

Connerney, J. E. P., et al., Jupiter's Magnetosphere and Aurorae Observed by the Juno Spacecraft During its First Polar Orbits, Science, Volume 356, Issue 6340, Pg. 826-832, May 26, 2017

Dawson, D., et al., Course 228, Module 4, Radiation Damage to Materials, June 02, 1993

Dedgaonkar, V. G., Sarwade, D. B., Radiation Effects on Thermal Decomposition of Ammonium Perchlorate, Journal of Radioanalytical and Nuclear Chemistry, Letters 165 (5), Pg. 269 – 275, 1992

Dedgaonkar, V. G., Navle, P. B., Shrotri, P. G., Diol-Diisocyanate Polymerization by Gamma Irradiation, Journal of Radioanalytical and Nuclear Chemistry, Vol. 176 (1), Pg. 77-84, July 1993

Dedgaonkar, V. G., et al., Properties of Hydroxy-Terminated Polybutadiene-based Elastomers under the Influence of Gamma Radiation, Journal of Radioanalytical and Nuclear Chemistry, Volume 173(2), Pg. 153-160, August 1993

Dedgaonkar, V. G., et al., Radiation Effects on Aging Behavior of Oligobutadiene-base Urethane Polymer, Radiation Physics and Chemistry, 48(3), Pg. 333-335, September 1996

Dessler, A. J., Physics of the Jovian Magnetosphere, Cambridge University Press, UK, 1983

Desmond, K. W., Weeks, E. R., Influence of Particle Size Distribution on Random Close Packing of Spheres, Physical Review, Number 90, August 22, 2014

Dickinson, J. T., Electron Bombardment Induced Crack Initiation and Crack Growth in Polymers and Polymer Surfaces, Adhesives, Sealants and Coatings for Space and Harsh Environments, Plenum Press, NY, 1988

Dongyuan, L., et al., The Effect of Radiation Cross-linking on the Mechanical Properties of Polyethylene Sheets, International Journal of Radiation Applications and Instrumentation, Part C, Radiation Physics and Chemistry, December 1987

Drake, F. D., et al., Non-thermal Microwave Radiation from Jupiter, Astronomical Journal, Volume 64, Pg. 329, 1959

Drobny, G. J., Ionizing Radiation and Polymers, 1st Edition, Principles, Technology, and Applications, Plastics Design Library Handbook Series, November 29, 2012

Egwaikhide, A. P., et al., Rheological and Mechanical Properties of Natural Rubber Compounds Filled with Carbonized Palm Kernel Husk and Carbon Black, Science Journal of Chemistry, Volume 1(5), Pg. 50-55, October 20, 2013

Einstein, A., Eine neue Bestimmung der Moleküldimensionen, Ann. Phys., vol. 19, pp. 289-306, 1906

Einstein, A., Investigation of Theory of Brownian Motion, Dover, NY, 1956

Engelhart, D. P., et al., Effect of Electron Bombardment on Polyimide Film, National Research Council at (US) Air Force Research Lab, Trans Tech Publications, Switzerland, 2018

Ennis, C. P., Kaiser, R. I., Mechanistical Studies on the Electron-Induced Degradation of Polymethylmethacrylate and Kapton, Physical Chemistry and Chemical Physics, September 30, 2010

Eringen, A. C., et al., Mechanics and Chemistry of Solid Propellants, Proceedings of the Fourth Symposium on Naval Structural Mechanics, Elsevier, Inc., 1967

Evans, D., Morgan, J. T., A Review of the Effects of Ionizing Radiation on Plastic Materials at Low Temperatures, Advances in Cryogenic Engineering Materials, Plenum Press, NY, 1982

Farris, R. J., The Character of the Stress-Strain Function for Highly Filled Elastomers, Journal of Rheology, Transactions of the Society of Rheology, Volume 12, Issue 2, July 24, 2000

Fleminert, G., Bueche, C., Light Reinforcement Filler, a paper presented to the Swedish Institute of Rubber Technology, 1957

Flory, Paul J., The Molecular Theory of Rubber Elasticity (re-published), Polymer Journal, Volume 17, Pg. 1-12, January 15, 1985

FS-2002-10-080-JSC, NASA Facts Understanding Space Radiation, NASA Lyndon B. Johnson Space Center, October 2002

Fletcher, W.P., Gent, A. N., Dynamic Shear Properties of Some Rubber Like Materials, British Journal of Applied Physics, Volume 8, Number 5, 1953

Foust, J., NASA Selects 9 Instruments for Europa Mission, Spacenews, May 26, 2015

Fu, Shao-Yun, et al., Effects of Particle Size, Particle/Matrix Interface Adhesion and Particle Loading on Mechanical Loading on Mechanical Properties of Particulate – Polymer Composites, Composites Part B: Engineering, Volume 39, Issue 6, Pages 933-961, September 2008

Garrett, H. B., Divine, N., The Jovian Charging Environment and its Effects, The Jet Propulsion Lab, California Institute of Technology, 2010, a review of the original work on Charged Particle Distributions in Jupiter's Magnetosphere, Journal of Geophysical Research, Vol. 88, No. A9, Pages 6889-6903, September 01, 1983

Geubelle, P. H., et al., Multiscale Modeling of Dewetting Damage inn Highly Filled Particulate Composites, 9th International Conference on Multiscale and Functionally Graded Materials – Proceedings of the International Conference, Volume 973, Pg. 196-202, March 13, 2008

Ghobashy, M., Abdeen, Z., Radiation Crosslinking of Polyurethanes: Characterization by FTIR, TGA, SEM, XRD, and Raman Spectroscopy, Journal of Polymers, Hindawi Publishing Corporation, October 5, 2016

Gligorijevic, N., et al., Mechanical Properties of HTPB Composite Propellants in the Initial Period of Service Life, Scientific Technical Review, 2014, Volume 64. No. 4, 2014.

Gligorijevic, N., et al., Mechanical Characterization of Composite Solid Rocket Propellant Based on Hydroxy-Terminated Polybutadiene, Military Technical Institute, Belgrade, Serbia, 2015

Goodier, J. N., Journal of Applied Mechanics, volume 55, 1933

Gross, J. H., Mass Spectrometry, Springer, New York, 2004

Guth, E., Mark, H. F., Intramolecular Statistics, Monatsh, Volume 93, Pg. 65, 1934

Haque, A.K., et al., Ch. 18 Electron Impact Atomic and Ionic Ionization: Analytical, Semiempirical, and Semiclassical Methods, Advances in Quantum Chemistry, Vol. 73, Pg. 363-414, 2016

Hareesh K., Ganesh, S., Eight MeV Electron Induced Changes in Structural and Thermal Properties of Lexan Polycarbonate, Materials Sciences and Applications, Volume 2, Pg. 1682-1687, November 2011

Hemmerich, Karl J., Polymer Materials Selection for Radiation Sterilized Products, Radiation Sterilization, Nelson Laboratories, February 01, 2000

Hepburn, C., Filler Reinforcement of Rubber, Journal of Plastic and Rubber International, Volume Number 9, Pg. 11-15, 1984

Hermans, J. J., Deformation and Swelling of Polymer Networks Containing Comparatively Long Chains, Laboratory for Cellulose Research of the AKU and Affiliated Companies, Utrecht, Communication Number 33, Holland, May 06, 1946

Hu, Y., et al., Modification of Carbon Nanotube-polystyrene matrix composites through polyatomic-ion beam deposition: predictions from molecular dynamics simulations, Composites Science and Technology 63, 2003

ICRU (1984). International Commission on Radiation Units and Measurements. ICRU Report 37, Stopping Powers for Electrons and Positrons.

Ide, K. M., Ho, S. Y., Fracture Behavior of Accelerated Aged Solid Rocket Propellants, Journal of Materials Science, Volume 34, Pg. 4209-4218, 1999

Inglis, H. M., et al., Cohesive Modeling of Dewetting in Particulate Composites: Micromechanics vs. Multi-scale Finite Element Analysis, Mechanics of Materials, Volume 39, Pg. 580-595, 2007

Inglis, H. M., Modeling the Effect of Debonding on the Constitutive Response of Heterogeneous Materials, Doctoral Dissertation, University of Illinois at Urbana-Champaign, 2014

Ito, M., Application of Chemo rheology to Radiation Damage of Elastomer, International Journal of Radiation Applications and Instrumentation, Part C, Radiation Physics and Chemistry, December 1988

Jablonski, A., et al., NIST Electron Elastic-Scattering Cross-Section Database, Version 3.2, NIST Standard Reference Database 64, US Department of Commerce, Gaithersburg, MD, December 2010

James, H. M., Guth, E., Theory of Elastic Properties of Rubber, the Journal of Chemical Physics, 1943

James, H. M., Statistical Thermodynamics of Rubber Elasticity, the Journal of Chemical Physics 21, Pg. 1039, 2004

JANNAF-PC, Solid Propellant Mechanical Behavior Manual, Chemical Propulsion Information Agency Publication 21, Joint Army-Navy-NASA-Air Force Propulsion Committee, Interagency Chemical Rocket Propulsion Group, 1988

Joseph, K., et al., Polymer Composites: Volume 1, First Edition, Wiley VCH Verlag GmbH & Co, KGaA, 2012

Jung, G. D., et al., A Three-Dimensional Nonlinear Viscoelastic Constitutive Model of Solid Propellant, International Journal of Solids and Structures, Volume 37, Issue 34, Pg. 4715-4732, August 22, 2000

Kerner, E. H., Proceedings from the Physical Society, volume B69, 1956

Kishore, K., et al., Mechanism of Oxidative Degradation of Binder During the Aging of Composite Solid Propellant, Journal of Applied Polymer Science, Volume 24, 1979

Kishore, K., Sridhara, K., Condensed Phase Behavior of Ammonium Perchlorate-Based Solid Propellants, Solid Propellant Chemistry, Defense Research & Development Organization, Ministry of Defense, New Delhi, 1999

Kitson, F. G., et al., Chapter 1- What is Gas Chromatography / Mass Spectrometry? A practical Guide, Pg. 3-23, Academic Press, 1996

Klager, K., Wrightson, J. M., Recent Advances in Solid Propellant Binder Chemistry, Mechanics and Chemistry of Solid Propellants, Proceedings of the Fourth Symposium on Naval Structural Mechanics, Pg. 47-74, 1967

Kornacka, Ewa M., Chapter 8- Radiation Induced Oxidation of Polymers, Applications of ionizing Radiation in Materials Processing, Institute of Nuclear Chemistry and Technology, Warsaw, Poland, 2017

Kratky, O., Porod, G., Diffuse Small Angle Scattering of x-rays in Colloid Systems, Institute for Theoretical and Physical Chemistry, The University of Graz, Journal of Colloid Science, Volume 4, Issue 1, February 1943

Kuhn, W., Uber die Gestaltfadenformiger Molekule in Losungen (On the Shape of Filiform Molecules in Solutions), Kolloidzeitschrift 68, Pg. 2, 1934

LaBel, K. A., Space Radiation Effects on Electronics: Simple Concepts and New Challenges, Materials Research Society, Fall Meeting, Boston, MA, November 29, 2004

Lapin, S. C., Modification of Polymer Substrates Using Electron Beam-Induced Graft Copolymerization, PTC Engineering Systems, LLC, RadTech International North America, Peterson Publications, 2014

Lopez, L. C., et al., Electron Beam Effects on Polymers, Mechanical and Thermal Properties of Electron Beam-Irradiated Poly (Phenylene Sulfide), Journal of Applied Polymer Science, February 20, 1989

Mahanta, A. K., Pathak, D. D., HTPB Polyurethane: A Versatile Fuel Binder for Composite Solid Propellant, Ch. 11, INTECH, 2011

Masayuki, Ito, Degradation of Elastomers by Heat and / or Radiation, Japan Atomic Energy Research Institute, Nuclear Education center, 2-28-49, M. Ito JAERI-Conference 95-003, 2007

Matonis, V. A., Small, N. C., A Microscopic Analysis of Composites Containing Layered Spherical Inclusions, Polymer Engineering & Science, March 1969

Matous, K., et al., Multiscale Modeling of Solid Propellants: From Particle Packing to Failure, Composites Science and Technology, Volume 67, P. 1694-1708, 2007

Mauk, B. H., et al., Energetic Ion Characteristics and Neutral Gas Interactions in Jupiter's Magnetosphere, Journal of Geophysical Research, Space Physics, July 17, 2004

McGeary, R. K., Mechanical Packing of Spherical Particles, Journal of the American Ceramic Society, October 1961

Merlette, N., Pagnacco, E., Structural Dynamics of Solid Propellants with Frequency Dependent Properties, Proceedings of the 12th European Conference on Space Structures, Materials 7 Environmental Testing, Noordwyk, the Netherlands, March 20, 2012

Miloshevsky G., et al., Materials Degradation in the Jovian Radiation Environment, NASA Marshall Space Flight Center, Huntsville, AL, 2017

Mishra, R., et al., Effect of Electron Irradiation on Polytetrafluoroethylene, Journal of Radiation Measurement, Volume 37(3), Pg. 247-251, June 2003

Mooney, M., A Theory of Large Elastic Deformation, Journal of Applied Physics, 11(9), Pg. 582-592, 1940

Mooney, M., the Viscosity of a Concentrated Suspension of Spherical Particles, Journal of Colloid Science, Volume 6, Page 162, 1951

Morrell, G., Pinns, Murray L., Effect of Oxidizer Particle Size on Solid Propellant Combustion Stability, NASA Technical Note (NASA TN D-2736), Lewis Research Center, Cleveland, OH April 1965

NASA SP-8053, Nuclear and Space Radiation Effects on Materials, NASA Space Vehicle Design Criteria, NASA Marshall Space Flight Center, 1970

Nicolasis L., Narkis, M., Polymer Engineering Science, volume 11, 1971

Nielsen, L. E., Landel, R. F., Mechanical Properties of Polymers and Composites, 2nd Edition, Marcel Dekker, New York, 1994

Normand, E., Radiation Effects in Spacecraft and Aircraft, NASA Goddard Space Flight Center, February 09, 2000

Odijk, T., Stiff Chains and Filaments under Tension, Macromolecules, Volume 28, Pg. 7016, 1995

O'Donnell, J., Whittaker, A. K., A Solid-State 13C-NMR Study of Crosslinking in Polybutadiene by gamma Radiation: Effect of Microstructure and Dose, Journal of Polymer Science, Part A, Polymer Chemistry 30(2), Pg. 185-195, February 1992

Olivani, A., et al., Aluminum Particle Size Influence on Ignition and Combustion of Ammonium Perchlorate – Hydroxyl Terminated Polybutadiene – Aluminum Solid Rocket Propellants, Advances in Rocket Performance Life and Disposal, Aalborg, Denmark, September 23-26, 2002

Pandya, C. V., et al., Differential Scattering Cross Sections for Elastic Electron-Magnesium Scattering, Romanian Journal of Physics, Volume 56, Numbers 1-2, Pg. 172-176, Bucharest, 2011

Payne, A. R., The Dynamic Properties of Carbon Black-loaded Natural Rubber Vulcanizates, Part I, Journal of Applied Polymer Science #6, pp 53-57, 1962

Pearce, E. M., et al., The Molecular Theory of Rubber Elasticity, expansion of the original work of Paul J. Flory, Contemporary Topics in Polymer Science at Plenum Press, New York, 1977

Phillips, E. M., New Developments in High Energy Electron Beam Induced Long Chain Branched Polyolefins for Low Density, Non-crosslinked Foams, E-Beam Services, Inc. Cranbury, New Jersey, 2017

Pukansky, B., Voros, G., Composite Interfaces, volume 1, 1993

Quemada, D., Rheologica Acta, volume 16, 1977

Radiation Applications Incorporated (RAI), Radiation Induced Solid Propellant Decomposition, Final Technical Report #347, Contract AF 49(638)-1125, Propulsion Division, Office of Aerospace Research, Air Force Office of Scientific Research, Long Island City, NY January 15, 1965

Ranogajec, F., et al., Improvement of the Polymer Properties by Radiation Grafting and Crosslinking, Polimeri, Institut Ruder Boskovic, April 29, 2009

Rempp, P., Franta, E., Grafting and Branching of Polymers, Centre de Recherches sur les Macromolecules, Strasbourg, France, 1971

Rivlin, R. S., Large Elastic Deformations of Isotropic Materials, IV, Further Developments in the General Theory, Philosophical transactions of the Royal Society of London, Series A, Mathematical and Physical Sciences, 241 (835), Pg. 379-397, 1948

Rogers, John H., the Giant Planet Jupiter, Cambridge University Press, UK, 1995

Romanova, V. A., et al., The Influence of the Reinforcing Particle Shape and Interface Strength on the Fracture Behavior of a Metal Matrix Composite, Acta Materialia, Volume 57, Issue 1, Pages 97 -107, January 2009

Sakai, T., Isihara, A., On the Elastic Theory of Rubber-like Elasticity, Faculty of Science, Tokyo University, Tokyo, Japan, June 28, 1948

Sanli, L. I., Gursel, S. A., Synthesis and Characterization of Novel Graft Copolymers by Radiation Induced Grafting, Faculty of Engineering and Natural Sciences, Sabanci University, Istanbul, Turkey, 2008

Sato, Y., Furukawa, J., A Molecular Theory of Filler Reinforcement Based upon the Concept of Internal Deformation, Rubber Chemistry & Technology, Volume 36, No. 4, Pg. 1081-1106, September 1963

Seltzer, S.M., et al., Electron Stopping Power & Range (ESTAR), National Institute of Standards (NIST), 2016;

Shaha, S., et al., Structural and Chemical Modification of Polymer Composite by Proton Irradiation, Avasthiba Department of Physics, University of Baroda, Vadodara, India, 2009

Shemansky, D. E., et al., A New Understanding of the Europa Atmosphere and Limits on Geophysical Activity, Astrophysical Journal, Volume 797, Issue 2, International Atomic Energy Agency, December 20, 2014

Shin S., Lee, S., The Influence of Electron Beam Irradiation on the Chemical and Structural Properties of Medical Grade Polyurethane, Ewha Medical Research Institute, School of Medicine, Ewha Women's University, Seoul, Korea, 2013

Singh, N. L., et al., Effect of ion Beam Irradiation on Metal Particle Doped Polymer Composites, Bulletin of Materials Science, Volume 34, No. 1, Pg. 81-88, Indian Academy of Sciences, February 2011

Smith, S. B., et al., Overstretching B-DNA: The Elastic Response of Individual Double Stranded and Single Stranded DNA Molecules, Science 271, Pg. 795, 1996

Soo Yun, K., et al., Viscoelastic Constitutive Modeling of Solid Propellant with Damage, International Journal of Solids and Structures, Volume 80, Pg. 118-127, February 2016

Spadaro, G., et al., Ionizing Radiation-Induced Crosslinking and Degradation of Polymers, Chapter 7, Applications of ionizing Radiation in Materials Processing, Universita degli Studi di Palermo, Palermo, Italy, 2017

Sparks, W. B., et al., Active Cryovulcanism on Europa? Astrophysical Journal Letters, Volume 839, Issue 2, International Atomic Energy Agency, April 20, 2017

Tappan, A., Heller, M., Europa Lander Material Selection Considerations, Sandia National Lab, Albuquerque, NM January 10, 2017

Stein, R., Tobolsky, A. V., an Investigation of the Relationship between Polymer Structure and Mechanical Properties, Part I: Relationship between Structure, Mechanical Properties, and Birefringence, April 01, 1948

Sternheimer, R. M. (1952), the density effect for the ionization loss in various materials, Phys. Revision 88, Pg. 851, 1952

Sternheimer, R. M., Seltzer, S. M., and Berger, M.J., Density effect for the ionization loss of charged particles, Phys. Revision B26, Pg. 6067, 1982

Valavala, P. K., Odegard, G. M., Modeling Techniques for Determination of Mechanical Properties of Polymer Nanocomposites, Review of Advanced Material Science, Volume 9, 2005

Vollenberg, P., et al., Particle Size Dependence of the Young's Modulus of Filled Polymers: 2. Annealing and Solid State Nuclear Magnetic Resonance Experiments, Polymer, 30 (9), Pg. 1663-1668, January 01, 1989

Watts, John W., Burrell, M. O., Electron & Bremsstrahlung Penetration and Dose Calculation, NASA- Marshall Space Flight Center, AL, June 1971

Williams, David R., Missions to Jupiter, NASA- Lunar & Planetary Science, Space Science Data Coordinated Archive, August 31, 2017

Xu, F., et al., Constitutive Modeling of Solid Propellant Materials with Evolving Microstructural Damage, Journal of the Mechanics and Physics of Solids (56), Pg. 2050-2073, 2008

Yan, D., et al., Effect of Long Chain Branching on Rheological Properties of Metallocene Polyethylene, Polymer Journal Volume 40, Pg. 1737-1744, 1999

Yang, X., et. al., Mechanical Properties Experimental Investigation of HTPB Propellant after Thermal Accelerated Aging, 5th International Conference on Computer-Aided Design, Manufacturing, Modeling and Simulation, American Institute of Physics, Conf. Proceedings (1834), 2017

Youssef, H. A., et al., Effect of Ionizing Radiation on the Properties of Acrylonitrile Butadiene Rubber/Clay Nanocomposites, Journal of Elastomers & Plastics, Volume 45, Pg. 407-428, February 26, 2015

Zamaniana, M., et al., Fracture Toughness of Epoxy Polymer Modified with Nano-silica Particles: Particle Size Effect, Engineering Fracture Mechanics, Volume 97, Pg. 193-206, January, 2013

Ziaie, F., et al., Dose Rate Effect on LDPE Cross-linking Induced by Electron Beam Irradiation, Nukleonika, 50(3), 125-127, 2005

Appendix A: Glossary

Ammonium Perchlorate (NH_4ClO_4): inorganic compound soluble in water used as a powerful oxidizer in commercial solid propellant applications. The white or colorless powder requires considerable safety precautions as a Class 4 oxidizer that can undergo an explosive reaction for particle sizes over 15 micrometers and is classified as an explosive for particle sizes less than 15 micrometers.

Ammonium Sulfate $(NH_4)_2SO_4$: inorganic salt commonly used as a fertilizer with high water solubility. In this dissertation, it is used as a substitute to ammonium perchlorate to render to achieve an inert but representative mixture of surrogate propellant.

Analysis of Variance: statistical methodology used to analyze the differences among group means in a sample set. In this dissertation, ANOVA is used to determine which ingredient or ingredients has greater effect on measured values of Y_{stress} and Y_{strain}.

Aziridine (C_2H_5N)**:** HX-752 functions as a crosslinker and bonding agent for resins and adhesives to improve strength and flexibility, solvent resistance, alcohol and water resistance. HX-752 improves hardness and adhesion to difficult substrates.

Binder: rubbery material that when cured forms the propellant matrix. Typically, it is augmented with chemical additives that create a network of crosslinks enabling the matrix to suspend a high concentration of solid particles corresponding to fuel and oxidizer.

Bremsstrahlung: electromagnetic radiation produced by a sudden slowing down or deflection of charged particles (especially electrons) passing through matter in the vicinity of the strong electric fields of atomic nuclei.

Carbon Black: a material produced by the incomplete combustion of heavy petroleum products that is used as a reinforcing filler in tires and other tuber products.

Chain Extender: extends the chain length of the hard segment effectively increasing the density of the hydrogen bond and the molecular weight of the matrix. The resulting connections contribute to the mechanical properties of the propellant.

Chain Scission: a chemical reaction that results in the breaking of skeletal bonds resulting in degradation of the polymer chain. The resulting break occurs at a random point in the backbone to form two fragments.

Class 4 Oxidizer: an oxidizer that causes a significant increase in the burning rate of the combustible material that they come in contact with and can undergo an explosive reaction due to contamination, thermal or physical shock.

Crosslinks/Crosslinking: a bond that connects one polymer chain to another leading to a network of connections. These links may take the form of covalent bonds or ionic bonds. The resulting network of connections leads to a change in physical properties.

Crosslink Density: The number of chemical crosslinks per unit volume in a polymer.

Curing: refers to the crosslinking of thermosetting resins whereas vulcanizing is normally analogous to rubbers.

Deflagration: outward propagation of the combustion sequence at subsonic speed.

Displacement: The result of the transfer of sufficient kinetic energy by an electron to an atom in the matrix causing it to be ejected from its equilibrium position.

Elastic Scattering: the process whereby the kinetic energy of a particle is conserved during an interaction with an atom in the matrix but the direction of propagation is modified.

Electron Bombardment: The process where a beam of electrons interacts with them matrix leading to changes in material properties. Electron bombardment can originate from manmade devices for experimental purposes or from celestial interaction due to the presence of electrons in space and being accelerated by Jupiter's magnetosphere.

Europa: One of the Galilean moons of Jupiter having an icy crust believed to be harboring an ocean beneath its surface and potentially capable of sustaining some forms of life.

Excitation: the addition of a discrete amount of energy (referred to as excitation energy) to a nucleus, atom or molecule resulting in its alteration, typically from the lowest energy state (ground state) to one of higher energy (excited state).

F Statistic (ANOVA): a value used to determine if the means between two populations are significantly different. It is used in combination with the p value when deciding if the overall results are significant. The F-value in the ANOVA test also determines the P value.

Gassing (off-gassing): In hydrogen compounds, the result from disruption of the bond structure leading to the release of the hydrogen molecule causing changes in material properties.

Grafting: the addition of polymer chains onto a surface.

Hybrid: inert material representative of solid propellant with all ingredients present with the exception of the ammonium perchlorate. Typically, casted with 18.5w% to 19w% aluminum particulate.

Hydroxyl-terminated Polybutadiene: an oligomer of butadiene terminated at each end with a hydroxyl functional group. It reacts with isocyanates to form polyurethane polymers. While HTPB can have multiple industrial applications, it is commonly used by the propellant industry to bind the oxidizing and fuel with other ingredients to form a solid but highly elastic material with rubbery characteristics.

Ionization: The process by which an atom or a molecule acquires a negative or positive charge by gaining or losing electrons to form ions typically in conjunction with other chemical changes. Ionization is typically the result of a loss of an electron after colliding with an external energetic electron, collisions with other atoms, molecules and ions.

Ionizing Radiation: Ionizing radiation is mechanisms where charged particles or x-rays interact with a material to strip electrons from the outermost orbital locations of the atoms in the material, effectively creating charged ions. In turn, this ionization disrupts the bonds in the material. The resulting electrons that are stripped during these primary interactions have sufficient energy to continue to create additional damage through a cascading mechanism in the material.

Isophorone Diisocyanate ($C_{12}H_{18}N_2O_2$): is used in the chemical synthesis of aliphatic polyisocyanates and polyurethanes and functions as a curing agent and hardener giving the propellant elastomeric properties with exceptional handling. It is a clear liquid with

a pungent odor and a molecular weight of 222.28 gm/mol. The handling of IPDI requires considerable safety precautions as it presents skin and respiratory hazards when handling it.

Jovian Environment: The region in space characterized by the presence of the planet Jupiter and its moons. The Jovian system has been observed as having a magnetosphere with trapped high energy particle belts representing significant radiation hazards to missions that continue to explore it.

Long-chain branching: the process by which polymer chains are joined without forming a complete network of chains.

Magnetosphere: the cavity created in the solar wind by Jupiter's magnetic field. It extends up to seven million kilometers in the Sun's direction, almost reaching the orbit of Saturn in the opposite direction. Jupiter's magnetosphere attracts and accelerates subatomic particles creating intense radiation belts that are much stronger than Earth's Van Allen Belts and as a result, create significant hazards to spacecraft.

Matrix: synonymous with HTPB binder. The rubbery material that suspends the fuel and oxidizer particles. It is typically casted using a mixture of plasticizer, curing agent, stabilizer, and cross-linking agent.

Methyl aziridine (C_3H_7N): serves as a bonding agent in the propellant mixture with a molecular weight of 57.096 gm/mol.

Monte Carlo Method: a computational algorithm that relies on repeated random sampling to obtain numerical results.

P-value: in ANOVA, the P-value is determined by the F-statistic and is the probability the results could have happened by chance.

Polymethyl methacrylate $(C_5O_2H_8)n$: a common thermoplastic used as a chain extender in solid propellant applications.

Polyol: an organic compound containing multiple hydroxyl groups. A molecule with more than two hydroxyl groups is a polyol, with a three a triol and with four a tetrol.

Propellant (R45): Propellant mixed with R45 resin characteristic of HTPB propellant base. R45 propellant is designed to enable a high concentration of aluminum and ammonium perchlorate particles to be added and suspended in the matrix.

Secondary Radiation: radiation that is emitted by molecules or atoms after bombardment by an initiating (primary) form of radiation. Initiating forms of radiation can consist of electrons, protons or photons of energy.

Surrogate: inert substitute for ammonium perchlorate consisting of ammonium sulfate (salt). This enables the mix to be casted and tested without the risk of inadvertent explosion.

van der Waals Force: a force dependent on the interaction between atoms or molecules that do not result in chemical – electronic bonding.

Appendix B: Application of Monte Carlo Method for Incremental Dose Determination

Monte Carlo simulation was used to estimate the relationship between the results for unirradiated specimens (0 Mrad) and the irradiated specimens (6 Mrad) as shown in Figures 5.2 through 5.7 of this dissertation. The Monte Carlo method is based on the generation of multiple trials to determine the expected value of a random variable. This method is based on the following probability function,

$$\Pr\left\{\left|\frac{1}{N}\sum_N \varepsilon - \mu\right| < \frac{3\sigma}{\sqrt{N}}\right\} \approx 99.8\% \qquad \text{B.1}$$

Where the error is represented by the term,

$$\varepsilon = \frac{3\sigma}{\sqrt{N}} \qquad \text{B.2}$$

with σ representing the standard deviation of the random variable and N is the number of iterations. Beginning with the known values at 0 and 6 Mrad, Monte Carlo simulations were developed in a spreadsheet format to obtain values for eleven increments between 0 Mrad and 6 Mrad as shown in Figures 5.2 through 5.7. In the case of Figure 5.2 (crosslink density from the Flory – Rehner method), thirteen increments were assigned to the dose in 0.5 Mrad increments with two of these increments having known values of 5.87E-05 mol/in^3 corresponding to 0 Mrad (unirradiated case) and 1.38E-04 mol/in^3 corresponding to 6 Mrad (irradiated case). The spreadsheet program was used to assign a standard error at these two points, which was determined graphically to be (+/-) 3.8E-05 mol/in^3 as shown below,

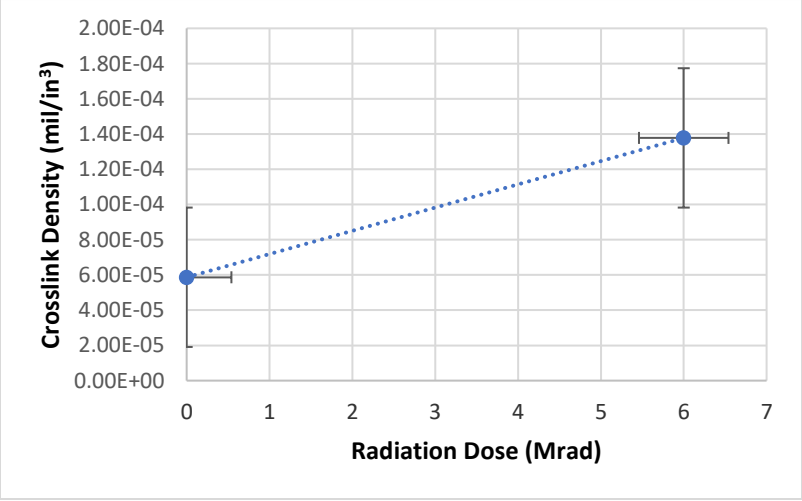

Figure B.1: Known Dose Points (w/ error assigned)

Each of the increments between 0 Mrad and 6 Mrad was assumed to have a crosslink density value between a minimum and a maximum. The error from the two known dose values was applied at 1.0 Mrad for the series of maximum values and at 5 Mrad for the series of minimum values to yield a set of graphs as follows,

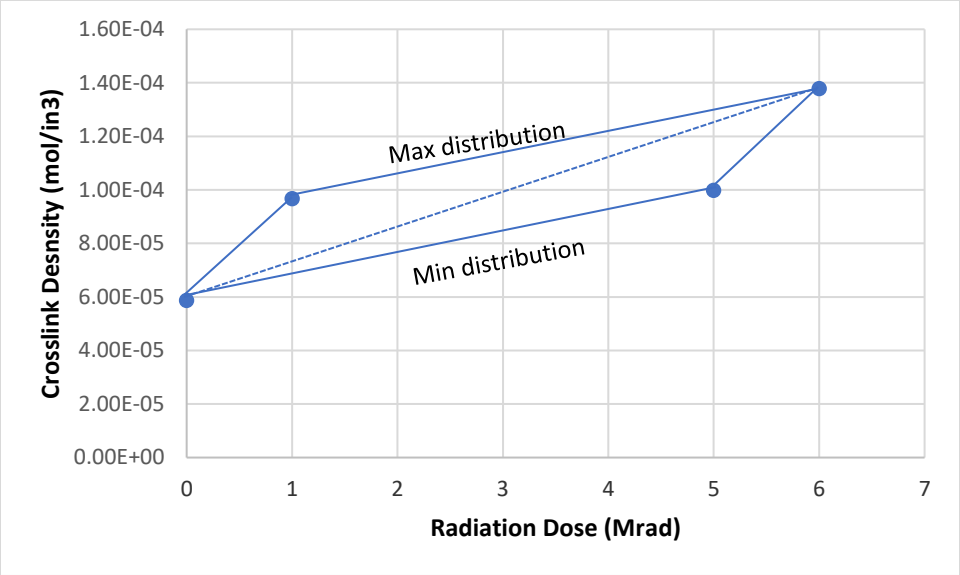

Figure B.2: Max & Min Crosslink Density Distributions

From this graphical representation the initial set of maximum and minimum values is shown below.

Table B.1: Initial Max and Min Crosslink Density Estimates

Dose (Mrad)	Min (mol/in^3)	Max (mol/in^3)
0	5.87E-05	5.87E-05
0.5	6.25E-05	8.00E-05
1.0	6.65E-05	9.67E-05
1.5	7.09E-05	1.04E-04
2.0	7.55E-05	1.08E-04
2.5	8.04E-05	1.11E-04
3.0	8.56E-05	1.15E-04
3.5	8.80E-05	1.18E-04
4.0	9.10E-05	1.22E-04
4.5	9.50E-05	1.29E-04
5.0	9.98E-05	1.32E-04
5.5	1.17E-04	1.34E-04
6.0	1.38E-04	1.38E-04

With an initial set of minimum and maximum values in place, a set of random numbers for each dose increment was determined using the RAND() function beginning with 0.5 Mrad as follows,

$$=\text{RAND}()*(8.0\text{E-}05 - 6.25\text{E-}05) + 6.25\text{E-}05 \qquad \text{B.3}$$

This formula generates a random value for crosslink density at 0.5 Mrad. Applying this relationship for the remainder of the ten increments yields a set of initial crosslink density values that needs to be repeated to achieve an error of less than 2%. To determine the number of iterations required to achieve an error of less than 2% it is first necessary to determine σ and $\mathcal{E}$ of the max and min values shown in Table B.1 for each dose increment. A standard spreadsheet program performs these functions with the use of the STDEVP command for standard deviation and the AVERAGE command. From the values in Table B.1, the number of iterations (N) required was 1,193 for each dose increment.

Because the computed crosslink density of 1.7E-04 mol/in^3 corresponding to the upper propellant value of Y_{stress} (173 psi) and Y_{strain} (65%) is above 1.38E-04 mol/in^3 at 6 Mrad, it became necessary to extrapolate the dose corresponding to the propellant upper crosslink density value. In conducting this extrapolation it was necessary to compute values for skewness using the SKEW command and Kurtosis using the KURT command in the spreadsheet program to assess the shape of the curve beyond 6 Mrad. The values computed for the crosslink density case suggested the distribution is somewhat flatter and to the right. Iterations of the Monte Carlo method for crosslink density, particle loading and debonding – adhesion provided an understanding of the benefits of the models as well as their constraints in relation to responding to a risk to the Europa mission.